NCA-LDAS: Overview and Analysis of Hydrologic Trends for the National Climate Assessment

MICHAEL F. JASINSKI*

Hydrological Sciences Laboratory, NASA Goddard Space Flight Center, Greenbelt, MD

JORDAN S. BORAK

Earth System Science Interdisciplinary Center, University of Maryland, College Park, MD

Hydrological Sciences Laboratory, NASA Goddard Space Flight Center, Greenbelt, MD

SUJAY V. KUMAR

Hydrological Sciences Laboratory, NASA Goddard Space Flight Center, Greenbelt, MD

DAVID MOCKO

Science Applications International Corporation, Beltsville, MD

Global Modeling and Assimilation Office, NASA Goddard Space Flight Center, Greenbelt MD

Hydrological Sciences Laboratory, NASA Goddard Space Flight Center, Greenbelt, MD

CHRISTA D. PETERS-LIDARD

Hydrosphere, Biosphere and Geophysics, Earth Science Division, NASA GSFC, MD

MATTHEW RODELL

Hydrological Sciences Laboratory, NASA Goddard Space Flight Center, Greenbelt, MD

HUALAN RUI

NASA Goddard Earth Sciences Data and Information Services Center, Greenbelt, MD

ADNET Systems, MD

HIROKO KATO BEAUDOING

Earth System Science Interdisciplinary Center, University of Maryland, College Park, MD

Hydrological Sciences Laboratory, NASA Goddard Space Flight Center, Greenbelt, MD

BRUCE E. VOLLMER

NASA Goddard Earth Sciences Data and Information Services Center, Greenbelt, MD

KRISTI R. ARSENAULT

Science Applications International Corporation, Beltsville, MD

Hydrological Sciences Laboratory, NASA Goddard Space Flight Center, Greenbelt, MD

BAILING LI

Earth System Science Interdisciplinary Center, University of Maryland, College Park, MD

Hydrological Sciences Laboratory, NASA Goddard Space Flight Center, Greenbelt, MD

JOHN D. BOLTEN

Hydrological Sciences Laboratory, NASA Goddard Space Flight Center, Greenbelt, MD

NATTHACHET TANGDAMRONGSUB

Earth System Science Interdisciplinary Center, University of Maryland, College Park, MD

Hydrological Sciences Laboratory, NASA Goddard Space Flight Center, Greenbelt, MD

Accepted May 30, 2019

---

*Corresponding author address: Michael F. Jasinski, Hydrological Sciences Laboratory, NASA GSFC, Code 617, Greenbelt, MD 20771

E-mail: Michael.F.Jasinski@nasa.gov

Abstract

Terrestrial hydrologic trends over the conterminous United States are estimated for 1980-2015 using the National Climate Assessment-Land Data Assimilation System (NCA-LDAS) reanalysis. NCA-LDAS employs the uncoupled Noah Version 3.3 land surface model at 0.125^{o}x0.125^{o} forced with NLDAS-2 meteorology, rescaled Climate Prediction Center precipitation, and assimilated satellite-based soil moisture, snow depth and irrigation products. Mean annual trends are reported using the nonparametric Mann-Kendall test at $p<0.1$ significance. Results illustrate the interrelationship between regional gradients in forcing trends, and trends in other land energy and water stores and fluxes. Mean precipitation trends range from +3 to +9 mm/yr in the Upper Great Plains and Northeast to -1 to -9 in the West and South; net radiation flux trends range from +0.05 to +0.20 W/m^2/yr in the East to -0.05 to -0.20 in the West; U.S.-wide temperature trends average about +0.03K/yr. Trends in soil moisture, snow cover, latent and sensible heat fluxes and runoff are consistent with forcings, contributing to increasing evaporative fraction trends from West to East. Evaluation of NCA-LDAS trends compared to independent data indicates mixed results. The RMSE of U.S.-wide trends in number of snow cover days improved from 3.13 to 2.89 days/yr while trend detection increased 11%; Trends in latent heat flux were hardly affected, RMSE decreasing only 0.17 to 0.16 W/m^2/yr, while trend detection increased 2%; NCA-LDAS runoff trends degraded significantly from 2.6 to 16.1 mm/yr while trend detection was unaffected. Analysis also indicated that NCA-LDAS exhibits relatively more skill in low precipitation station density areas, suggesting there are limits to the effectiveness of satellite data assimilation in densely gaged regions. Overall, NCA-LDAS demonstrates capability for quantifying physically consistent, U.S. hydrologic climate trends over the satellite era.

1. Introduction and Background

Numerous reports confirm that the climate of the conterminous United States (CONUS) has been changing over the past several decades (Melillo et al., 2014; USEPA, 2016; USGCRP, 2017b) consistent with overall North American trends (Blunden and Arndt Eds., 2013). Analyses of in situ temperature data indicate that current summers are longer and warmer compared to anytime in the past U.S. record, and that this trend has been accelerating over the past several decades (USGCRP, 2017b). Trends in annual means and extremes have been detected, with minimum temperatures increasing more than maximum temperatures (E.g. Lee et al., 2014; Peterson et al, 2008). Such warming is manifested in most components of the terrestrial hydrologic cycle, linked through land and atmospheric energy and water conservation dynamics. For instance, national trend summaries (USEPA, 2016; Melillo et al., 2014; USGCRP, 2017b) indicate increased annual precipitation (P) and streamflow throughout the Northeast and upper Midwest, and increasing flooding in rivers near inland cities (Walsh et al, 2014). Heavy precipitation events have increased (Melillo et al., 2014; Zhang 2011), especially in its eastern half. Decreasing snow trends have been identified in the Intermountain West (Harpold et al., 2012) and Southwest while increasing in the North (Kunkel et al., 2009, 2016). Between 1972 and 2015, the extent of North American snow cover decreased on average about 9,000 km^2/yr, largely in spring and summer, and the snow cover season has shortened by about two weeks (USEPA, 2016).

Assessments of national climate are coordinated by the U.S. Global Change Research Program (USGCRP) through the National Climate Assessment (NCA) (USGCRP, 2012; USGCRP, 2017a; USGCRP, 2017b; Melillo et al., 2014). The Global Change Research Act of 1990 calls for an NCA report to be produced on a quadrennial basis. The Third and

Fourth NCA had a significant focus on climate impacts in regions of the U.S. and sectors of the U.S. economy (Melillo et al., 2014; USGCRP, 2017b). Chapters reviewed climate change science and discussed adaptation (Bierbaum et al., 2014), mitigation (Jacoby et al, 2014), and decision support (Moss et al., 2014). USGCRP's NCA efforts fall under the "Conduct Sustained Assessment" goal identified in the USGCRP Strategic Plan (USGCRP 2012, 2017b); the focus is to "build sustained assessment capacity that improves the Nation's ability to understand, anticipate, and respond to global change impacts and vulnerabilities".

A specifically identified need of the NCA's Sustained Assessment is to develop consistent trend indicators that track and communicate the causes and effects of climate change, as well as the tools to analyze them (USGCRP, 2017a). Successful indicators provide a basic understanding of the physical system, quantify a state that can be tracked over time (USEPA, 2016) including its uncertainties, are easily interpreted by technical and non-technical users (Janetos et al., 2012), and are publicly accessible and documented.

Unfortunately, to date there has been limited capability in providing the above requirements at the nation-wide scale. Most trend studies rely on in situ data, and are usually focused on a specific region. Studies also differ over the time period of the analyses, or the reference period to which a particular trend is being compared (Melillo et al., 2014; USEPA, 2016; USGCRP, 2017b; Blunden and Arndt Eds., 2013; Lee et al., 2014; Peterson et al, 2008; Walsh et al, 2014), complicating their comparison with other studies. Further lacking is a publicly available, spatially consistent, database of the full suite of terrestrial energy and water related variables with analysis tools. This would facilitate comprehensive indicator analyses over all components of the land water and energy balance, while serving potential users in other related physical, biological and socioeconomic sciences.

In developing trends, there is also need to optimally merge all relevant data (Dee et al, 2011; 2014) including in situ and remotely sensed data products. For instance, despite a wealth of quality in situ point observations throughout the U.S., sparse in situ observations may not capture the complexity and spatial variability of a region. Further, time series observations can possess non-climatic jumps due to changes in station relocation or instrumentation (Aguilar et al., 2003), making it difficult to separate the natural climate variability from observation inhomogeneity (Kunkel et al., 2007).

Space-based observations offer spatially consistent environmental data records (EDRs), but present their own challenges for trend analysis. For example, optical multispectral sensors that observe land, water, and atmospheric properties, such as the Sentinel-2 mission, have daily to weekly coverage and pixels from 10 to 60m. SWE and soil moisture from microwave sensors such as the Advanced Microwave Scanning Radiometers (AMSR-E and AMSR-2) have daily to weekly coverage with 625 km^2 pixels. The Gravity Recovery and Climate Experiment mission sensors (GRACE and GRACE-FO) observe at about 250,000 km^2 resolution. Of additional concern are time series discontinuities associated with the short record length of individual missions usually designed for a 3 to 5-year lifecycle, bias between in situ and satellite observations (Dee et al., 2014), and data inhomogeneities associated with replacement and intercalibration between old and new sensors (Su et al., 2016).

Over the past decade, land reanalysis through satellite data assimilation has improved the estimation of gridded hydrologic time series, including variables not routinely measured, mainly by constraining stores and fluxes (Boni et al., 2001; Reichle et al., 2002). To date, most studies have focused on univariate satellite assimilation addressing soil moisture

(Galantowicz, 1999; De Lannoy et al., 2015), surface temperature (T) (Reichle et al., 2010), runoff (R) (Chen et al, 2014; Brocca et al., 2012), terrestrial water storage (Zaitchik et al., 2008; Forman and Reichle, 2013; Girotto et al., 2016), evapotranspiration or latent heat flux (ET) (Park and Choi, 2015; Peters-Lidard et al., 2011), snow cover and water equivalent (Slater and Clark, 2006; Zaitchik and Rodell, 2009), and vegetation (Barbu et al., 2014; Sawada and Koike, 2014; Sawada et al., 2015). Land data assimilation systems (LDAS) have further enabled regional to global reanalysis by imbedding simulations within sophisticated modeling environments. Examples include the North American LDAS (NLDAS-2) (Mitchell et al., 2004; Xia et al., 2012), the Global LDAS (GLDAS) (Rodell et al., 2004), the Famine Early Warning Systems Network LDAS (FLDAS) (McNally et al., 2017) which run within the NASA Land Information System (LIS) (Kumar et al., 2006). Other examples include LDAS-Monde (Albergel et al., 2017) and the Coupled Land and Vegetation DAS (CLVDAS) (Sawada and Koike, 2014; Sawada et al., 2015).

Although there has been considerable discussion on the value of satellite data assimilation within atmospheric models for climate analysis (Bengtsson et al., 2004; Dee et al, 2011; Albergel et al., 2013; Thorne and Vose, 2010; Grotjahn et al., 2018; Simmons et al., 2010; Dorigo et al., 2012), there have been comparatively few trend studies using land data assimilation (Girotto et al., 2017; Khaki et al., 2018; Khaki and Awange, 2019). Girotto et al. (2017) reported mixed results from GRACE assimilation within the Catchment model due to unmodeled processes, while Khaki and Awange (2019) reported improved ground water trends by assimilating GRACE and satellite soil moisture within the World Wide Water Resources Assessment model. Both studies identified the need for improved modeling of groundwater withdrawals.

NCA-LDAS was recently developed as a particular instance of LIS that includes a first-of its-kind assimilation of multi-sensor Earth observations of soil moisture, snow cover and depth, and irrigation simulation over the continental U.S. (Kumar et al., 2018). The long-term vision, shown in Figure 1, is to optimally combine the full suite of past and future Earth observations of all relevant land EDRs observations to provide high quality, publicly available data products and analyses that support the USGCRP's goals for sustained climate assessment (Jasinski et al., 2014; 2015).

NCA-LDAS's current products (https://ldas.gsfc.nasa.gov/NCA-LDAS) demonstrated high skills for soil moisture, snow depth, R and ET when compared to eight other land surface models (Kumar e al., 2018). NCA-LDAS time series of 42 land products thus offer one of the most compelling databases for constructing consistent, gridded national hydrologic trends. Example trends of the principal terrestrial components described herein demonstrate NCA-LDAS's flexibility as an enabling tool for investigating terrestrial hydrologic climate science and decision support.

2. Approach

a. Model Setup Summary

NCA-LDAS, summarized in Table 1 and Figure 2, employs the uncoupled Noah version 3.3 (Ek et al., 2003) at 0.125^{o}x0.125^{o} spatial resolution over the continental U.S., with a 36-year (1979-2015) record of NLDAS-2 forcings and satellite-based products. The precipitation field is derived from gauge-only Climate Prediction Center (CPC) analysis of daily precipitation (Higgins et al., 2000; Chen et al., 2008), with orographic adjustment (Daly et al., 1994). The meteorology forcing fields including surface temperature, radiation, wind,

and humidity are derived primarily from the North American Regional Reanalysis (Mesinger et al., 2006). The current NCA-LDAS Version 2.0 simultaneously ingests satellite-based EDRs of soil moisture, snow depth and cover, and irrigation intensity. Assimilation employs a 1-D ensemble Kalman Filter (Reichle et al.; 2002) with concurrent, sequential assimilation of satellite EDRs, while irrigation is simulated using a demand driven approach based on a MODIS classification scheme (Ozdogan et al., 2010; Kumar et al., 2018). Specific satellite platforms and corresponding EDRs assimilated into NCA-LDAS are listed in Table 2.

b. Trend Development and Assessment

Mean annual trend indicators of the principal terrestrial water cycle components for October 1979 through September 2015 (or water years 1980-2015) were computed using NCA-LDAS. Trends were constructed from NCA-LDAS daily data products and mapped for each grid cell in the domain. Analyses focused on monotonic trends in annual mean and standard deviation, and annual high and low multi-day averages using the nonparametric Mann-Kendall test (Mann, 1945; Kendall 1975; Helsel and Hirsch, 2002). For ease of comparison, the results were mapped at a common 10 percent significance level ($p<0.10$) except where noted. Grid cell values that did not pass the significance test were left blank. Trends were qualitatively compared to other published values, and also statistically evaluated for each NCA region with independent data for three land components (ET, number of snow-covered days (SCD) and R) using root mean square error (RMSE), or,

$$RMSE = \sqrt{\frac{\sum_{i=1}^{n} \left(Trend_{EVAL,i} - Trend_{NCA\_LDAS,i}\right)^2}{n}}$$

where $Trend_{NCA\_LDAS,i}$ is the estimated significant NCA_LDAS trend value a of grid cell i, $Trend_{EVAL,i}$ is the corresponding significant independent evaluation data trend in cell i, and n

is the total number of significant grid cell pairs. If either the NCA_LDAS or EVAL trend value was not significant for a given cell, the pair was not included in the RMSE calculation.

3. U.S. Terrestrial Hydrology Trend Indicators

a. Data assimilation impact vs. precipitation station density

Prior to computation of the indicators, an analysis was conducted to determine how well NCA-LDAS improves forecasts as a function of CPC precipitation station density. Precipitation is arguably the most important forcing in land surface models. Despite high quality gage observations, sparse sampling can impact the quality of the daily grid-cell estimate (Wilson et al., 1979; St-Hilaire et al, 2003; Krajewski et al., 2003; Villarini, 2008). CPC grid-box precipitation is estimated from the four reporting gages that are closest to the center of the cell using optimal interpolation. While there are typically about 8000 daily reporting stations over the continental U.S. (Chen et al., 2008), station density is not equally distributed as shown in Figure 3a (from Higgins et al., 2000). Average daily gage density for the NCA-LDAS grid cell is about 0.16 gages/cell, although the actual daily reporting density can be as low as zero. Lowest densities generally occur in the Southwest and Midwest.

The analysis was conducted by stratifying soil moisture, snow depth and streamflow skill as a function of the station density. Skill was estimated in terms of anomaly correlation, RMSE, and the Nash Sutcliffe Efficiency (NSE) normalized information contribution (NIC; Kumar et al., 2009) as compared to the open loop (OL) or non-data assimilation case, as reported in Kumar et al., 2018. While the number of stations reporting can vary overtime, only the average station density was used in the analyses. The range of station densities varied for each variable due to the availability of *in situ* data. Results are shown in Figures

3b, c and d for soil moisture, snow depth and streamflow, respectively. For soil moisture, anomaly correlations of NCA-LDAS compared to *in situ* data are generally higher than for the OL for all densities in the range of 0.0 to 1.0, except 0.8. Streamflow comparisons using NIC indicate that improvement is generally better where station density is lower than 0.8 but about the same for larger densities. In the case of snow depth, the RMSE is lower for NCA-LDAS compared to OL for all densities 0.8 or lower, but mixed for larger densities. These results suggest overall that NCA-LDAS improves skill and value when precipitation station density is low. They further suggest that there are possible limits to the effectiveness of data assimilation in regions with dense gage networks.

b. Precipitation

Given that NCA-LDAS is not dynamically coupled to an atmospheric model, trends were first derived for the P, net radiation (Rnet) and T forcing variables to understand their variability. For mean annual P, the trend is shown in Figure 4a for NCA-LDAS's full output, and also in Figure 4b for only $p<0.10$ significance. The results reveal that significance testing eliminates most of the coverage in Figure 4b, indicating that less than about one-third of the U.S. exhibits a non-zero P trend for $p<10$. Significant regions indicate increasing trends of 3 to 9 mm/yr for most of the Northeast stretching down into Ohio, Indiana, Illinois, and also in North Dakota and Montana. Decreasing trends of a similar magnitude are shown in Minnesota, while decreasing trends of -1 to -9 mm/yr are exhibited throughout the West and Southwest including Arizona, New Mexico, Nevada, southern Colorado and California. Decreasing trends of up to -10 mm/yr were computed for Oregon and Washington.

The above patterns and magnitudes from the NCA-LDAS trends are generally consistent with other published sources including the National Center for Environmental Information

(https://www.ncdc.noaa.gov/temp-and-precip/us-trends), and the USGCRP Fourth Assessment annual precipitation change, computed as the difference between the average annual present-day period (1986-2015) and the average annual baseline period (1901-1960) (See NOAA NCEI Figure 7.1, p. 209 in Easterling et al., 2017; analysis based on Peterson et al., 2013). However, exact comparison is problematic as: each analysis employs a different precipitation database (CPC vs Global Historical Climatology Network (GHCN)-Daily station data), different significance (p=0.1 vs 0.05) and reporting analysis (trends in mm/yr vs. change in percent); the NCA-LDAS time period does not extend prior to 1979; and the USGCRP does not report significance. Despite these differences, the NCA-LDAS, NCEI, and USGCRP show an increase in P of about 5-10% in the Northeast and Midwest and -5 to -10% in the Southwest over a 30-year period. The one exception is Northwest where NCA-LDAS shows decreasing trends while NOAA/NCEI change is increasing.

Several indicators representing precipitation variability also were developed. Figures 5a and 5b indicate trends in the annual mean number of days of heavy (> 10 mm) and very heavy precipitation (> 20 mm) at $p<0.10$, respectively, as described by Zhang et al. (2011). Trends in heavy precipitation range from about +1 to over +4 days per decade in the eastern U.S. with the greatest amounts in the northeast, to -1 to -4 days/decade in the southwestern and western states. Trends in very heavy precipitation cover a greater percentage of area but show slightly fewer number of days. Also plotted in Figure 5c and 5d are the annual trends in precipitation variance and in annual 5-day high precipitation, respectively. Trends in precipitation variance somewhat mirror those of heavy and very heavy precipitation; all three of which have a similar pattern with some regional differences. Indicators capturing the more extreme precipitation trends, including very heavy precipitation, variance, and 5-day

high, show increased trends along the Atlantic coast.

When comparing the annual and extreme trends, several features are noted. First, areas of increasing heavy precipitation and precipitation variance coincide with the regions of increasing annual P, as seen in the upper Great Plains, the Ohio River basin and the Northeast. Perhaps more noteworthy is that the area covered by the extreme indicators exhibiting increasing trends (Figures 5a,b,c,d) is much larger than that of the annual P trend in Figure 4b. The coverage of heavy precipitation also extends further into the southern U.S. Western U.S. areas of decreasing annual trends in P also show decreasing trends in extremes. These results suggest that while in many parts of the U.S. there is no significant trend in annual mean P as determined by the Mann-Kendall test, the distribution of the annual P is changing, with more intense individual rainfall events. More extreme P is evident along the U.S. Gulf and Atlantic Coasts, extending from Texas to Maine. These findings show overall good consistency with previous assessments (USEPA, 2016; Melillo et al., 2014; Karl et al., 2009).

c. Temperature

The NCA-LDAS mean annual T trend is shown in Figure 6a. Most of the trends computed over the northern Great Plains, northern Rockies and Intermountain West, and northwestern U.S. do not pass the significance test. The results show that for the period 1979 to 2015, the trend in annual mean T for most of the U.S. has been increasing at a CONUS-wide average of about 0.28 K/decade, while regionally ranging from -0.1 to +1.0 K/decade. The largest increases of 0.25 to 0.50 K/decade occur in the northern Midwest in upper Michigan and northern Wisconsin. T trends in the Southeast show a smaller increase of only 0.1 to 0.25 K/decade, with only slight changes along the Atlantic and Gulf Coasts, except for

Florida that exhibits negligible significant trend. Parts of the Southwest including Arizona, New Mexico and California also show an increasing trend of 0.1 to 0.5 K/decade. These NCA-LDAS results are generally consistent with NOAA NCDC changes between average present-day temperatures (1986-2016) and reference period averages (1901-1960) (Melillo et al., 2014), although NOAA shows a decreasing average T change in Alabama and Mississippi (Hausfather et al., 2016; Rohde et al., 2013) that is not supported by NCA-LDAS. NCEI national trends (https://www.ncdc.noaa.gov/temp-and-precip/us-trends), reported at $p<0.05$, are also consistent with NCA-LDAS with no significant trends reported in the Northwest and Northern Great Plains. The NCDC results also exhibit mostly increasing trends throughout the western U.S., although their significance levels were not reported.

d. Net Radiation

The trend in annual net downward radiation (Rnet) is often not reported, but it is nonetheless an important energy forcing as it impacts on trends in ET and other components of the land surface energy and water balance. Global Rnet trends over the past several decades have been analyzed with respect to trends in aerosols, cloud cover, and surface albedo. Analyses based on International Satellite Cloud Climatology Project data (Wild, 2012; Wild et al., 2008) indicate non-linear trends since the 1950s ranging from -1.0 to over +2.0 W/m^2/decade (E.g. Cohen and Stanhill, 2016).

The NCA-LDAS indicator for annual trend in Rnet is shown in Figure 6b. Results indicate a strong regional pattern with a distinct east-west trend gradient stretching across the U.S. A positive annual Rnet trend of about + 0.05 to 0.20 W/m^2/yr is estimated throughout most of the eastern half of the U.S., with greatest magnitude in the Southeast, ranging up to

319 0.25 W/m^2/yr. The Rnet trend gradient decreases to the West, with a low -0.05 to -0.20
320 W/m2/yr in the West and Southwest. A unique North-South swath through the Great Plains,
321 where the Rnet transitions from positive to negative, exhibits no significant trend. A notable
322 sharp decrease in Rnet in Wyoming is likely due to a disproportionately greater number of
323 precipitation stations in the mountainous areas compared to lower elevations. A slight
324 increase in Rnet is also shown in the Northwest, especially the coastal region of Oregon and
325 Washington. The above trends in the East are consistent with published results using a
326 combination of satellite data, reanalysis, modeling and GEWEX/SRB analyses (Cohen and
327 Stanhill, 2016; Ma et al, 2017; Niu et al, 2011) except for NCA-LDAS western decreasing
328 trends that are not supported.

329 ***e. Soil Moisture***

330 The indicator for NCA-LDAS annual soil moisture trends, shown in Figure 7, was
331 computed based on the total column moisture content within the four NCA-LDAS soil layers.
332 The results show consistency with annual P trends where significance is reported. That is,
333 there are positive soil moisture trends in the Northeast and upper Great Plains and northern
334 Rocky Mountains averaging up to 3 mm/yr. Decreasing trends in soil moisture cover most of
335 the remaining U.S., especially the Northwest, Southwest and upper Midwest, ranging from -1
336 to -9 mm/yr. Decreasing trends down to -3 mm/yr appear in Louisiana and Florida. The
337 overall NCA-LDAS U.S. drying trend in the West and Southwest is generally consistent with
338 trends developed from the merged global microwave-based surface soil moisture dataset of
339 the European Space Agency (ESA) Climate Change Initiative (CCI) (Feng and Zhang, 2015;
340 Dorigo et al., 2012; Liu et al., 2012). NCA-LDAS also shows drying across the southern
341 U.S. which is not generally supported in the SM-MW product.

f. Latent Heat Flux

The NCA-LDAS indicator for mean annual ET for 1980-2015 is shown in Figure 8a. Results show increasing trends throughout the eastern half of the U.S. and upper Midwest, with greatest magnitude in the South stretching from eastern Texas to northern Florida. The positive annual trends in the East are similar in distribution as Rnet trends previously shown in Figure 6b. There is also additional positive response to the increased P (Figure 4b) and Rnet throughout most of the northern U.S. Notable exceptions are southeast Texas, which exhibits a negative trend in ET compared to Rnet, while Florida exhibits mixed increasing and decreasing trends. Overall, from a climate standpoint, the East and North behave as energy limited systems.

In stark contrast to the eastern U.S., negative trends in ET extend throughout most of the West and Southwest. Trends ranging from -0.05 to -0.25 $W/m^2/yr$ are exhibited in nearly the same regions as the negative P (Figure 4b), Rnet (Figure 6b) and soil moisture trends (Figure 7). The strong decreasing ET trend with similar negative trends in soil moisture and P indicate a climatically moisture limited system. These results are consistent with previous NLDAS-2 analyses over the Missouri Basin, California, and Mexico, (Parr et al., 2016) that showed a strong positive correlation between ET, P and soil moisture, and a negative correlation with Rnet. However, NCA-LDAS trends differ to the Parr study by also exhibiting ET trends in the same direction as Rnet and T, where additional factors including soil moisture, land cover type, aerosols and cloud cover come into play.

The NCA-LDAS ET trends were statistically evaluated against the FLUXNET_MTE multi-tree ensemble (Jung et al., 2009) data product trends using RMSE. FLUXNET-MTE provides monthly, 0.5^{o}x0.5^{o} gridded ET, independently derived from upscaling eddy

365 covariance measurements from the FLUXNET global network (Baldocchi et al, 2001).
366 While not ground truth, it has been successfully used for benchmarking gridded surface
367 fluxes (E.g., Bonan et al., 2011; Alemohammad et al., 2017). The analysis was conducted
368 only for the period of overlap of the NCA-LDAS and FLUXNET-MTE data products, or
369 1983-2008, where grid cells from both datasets exhibited significance, as shown in Figures
370 8b and 8c. Visual inspection indicates generally good agreement between the NCA-LDAS
371 and FLUXNET trends throughout the U.S., except in the upper Midwest states of Illinois,
372 Wisconsin, Iowa and Minnesota, where the trends are opposed. Statistical results, aggregated
373 to each NCA region, are shown in Table 3. They indicate RMSE errors ranging from 0.05
374 $W/m^2/yr$ in the Northeast to 0.21 $W/m^2/yr$ in the Midwest, with a CONUS wide error of 0.16
375 $W/m^2/yr$.

376 ***g. Sensible Heat and Evaporative Fraction***

377 Trends were also developed for 1980-2015 for the mean summer, or June-July-August
378 (JJA), ET, the sensible heat flux (H), and mean evaporative fraction (EF), shown in Figures
379 9a, b and c, respectively. Overall, for this period, H trends are about one-third to one-fourth
380 the magnitude of the ET trends. There are decreasing trends from the Upper Great Plains to
381 the Intermountain West, and increasing trends in the Southeast and Northwest.

382 Trends in the mean JJA EF, where EF is the ratio of ET to total available energy flux or
383 EF=ET/(H + ET), are also computed, demonstrating low but positive values throughout the
384 entire East, then extending with increasing EF trend gradient toward the Upper Great Plains.
385 The NCA-LDAS estimated trends for the significant grid cells are greatest in the upper Great
386 Plains and upper Midwest about 0.03 EF/decade or 10.8% over the 36-year period. For these
387 regions, EF trends favor the production of ET, or an increase in ET. Trends become negative

388 moving into the Southwest decreasing down to 0.04 EF/decade or -14% in some regions.
389 The implication is that the Southwest is trending to increasingly drier conditions, while the
390 upper Great Plains are trending toward more temperate conditions.

391 ***h. Snow-Covered Days***

392 Several studies and reports have indicated that the number of annual SCD is decreasing
393 in the U.S. and North America (USEPA, 2016; Rutgers University Global Snow Lab, 2016;
394 Mote and Sharp, 2016). An NCA-LDAS indicator that depicts the trend in annual SCD is
395 shown in Figures 10a for the full 1980-2015 period. Results indicate decreasing trends
396 ($p<0.1$) across nearly the entire the U.S. ranging between 0 to over 2 days/yr, with the largest
397 decrease occurring in the West and Intermountain West. The mean annual CONUS-wide
398 trend is -1.2 days/yr, over twice published values (Hori et al., 2017; USEPA, 2016; Knowles,
399 2015; Burakowski et al., 2008) although there is high uncertainty due to varying methods and
400 data records. Possible reasons for this discrepancy are discussed in Section 4.a.

401 Also plotted in Figures 10b and c are a comparison of annual SCD trends estimated from
402 both NCA-LDAS and the gridded CMC snow depth product (Brown et al, 2010),
403 respectively, but only the period for which the CMC data are available or 1999-2015. During
404 these more recent 15 years, both figures indicate a strong decrease in SCD of more than 2
405 days per year especially in the central and northern Rocky Mountains. There is also some
406 agreement that during 1999-2015 the number of SCD has actually increased slightly in the
407 central U.S. However, area covered by significant trends for this abbreviated period is only
408 about one-third of the US, most likely due to the statistical effect of comparing the shorter
409 available 16-year record.

410 Two analyses were carried out to evaluate NCA-LDAS trends. First, the NCA-LDAS

411 SCD indicator was compared to earlier analyses by Harpold et al. (2012) over nine
412 watersheds covering a majority of the Intermountain West region shown in Figure 10a. They
413 analyzed trends in snow cover duration using SNOTEL data collected between 1984 and
414 2009, applying the regional Mann-Kendall test at $p<0.05$. Their results for each basin, shown
415 in Figure 10a, yielded significant negative trends ranging from 0.3 days per year in the upper
416 Colorado, to 0.9 days per year in southeast Utah. Also plotted on the same graph are the
417 NCA-LDAS SCD trends of only the model grid cells covering each watershed, adjusted for
418 the same period and $p<0.05$ value as the Harpold analysis. Results show very good
419 agreement in negative trend direction in 10 out of 13 basins analyzed, especially the Upper
420 Colorado. Of the three remaining watersheds, no comparison could be made as significance
421 was met in neither the NCA-LDAS nor Harpold analyses. NCA-LDAS trends generally
422 exhibited greater magnitude compared to Harpold's study by a factor of about 2. Potential
423 reasons for this Bias are discussed in Section 4a.

424 Second, similar to the above ET analyses, the RMSE was evaluated for NCA-LDAS
425 SCD trends, compared to the trends of an independent dataset, in this case the CMC snow
426 cover product or the overlapping period 1999-2015. Only those grid cells possessing a
427 significant trend in all three data products were used in the computation ($p<0.10$) as shown in
428 figure 10b and c. Analyses were conducted for each NCA region and for CONUS shown in
429 Table 3. They indicate RMSE errors ranging from 1.15 days in the Northeast to 2.51 days in
430 the Midwest, with a CONUS wide error of 2.9 days.

431 ***i. Snow Water Equivalent***

432 Trends in annual CONUS-wide snow water equivalent (SWE) based solely on
433 observations are difficult to estimate as the quantities available from station data are

primarily snow depth, precipitation, and temperature. Satellite-based SWE can be unreliable in complex terrain, forested areas, and in deep snow (Luojus et al, 2016) although regional evaluations exist (E.g. Mote and Sharp, 2016). This is due in large part to lack of knowledge of snow density, that needs to be estimated from snowfall and temperature (Knowles et al, 2015; Sturm et al, 2016). By merging both *in situ* snow data and satellite snow observations, NCA-LDAS is able to provide an estimate of CONUS-wide SWE at the grid cell resolution.

An indicator consisting of mean SWE for the snow season months of October through June at $p<0.1$ was developed as shown in Figure 12a. Results show a clearly defined region of decreasing trends in SWE over much of the southern and western U.S. Trends in the south are negative, but not hydrologically relevant. Increasing trends in SWE are identified in parts of the Northeast and in the northern to central Rocky Mountains.

The NCA-LDAS mean SWE indicator can be qualitatively compared to the trend in the National Operational Hydrologic Remote Sensing Center (NOHRSC) SNOw Data Assimilation System (SNODAS) data product for 2004-2015 which became available in 2003 (NOHRSC, 2004; Barrett, 2003). Recognizing the limitations of trend estimation over such a short period, the two data bases compare favorably as shown in Figures 12b and c, respectively. The significant areas are predominantly the West and Northwest where the estimated SWE annual trend ranges to -0.5 mm/yr. Computed significant trends for NCA-LDAS are also evident in the northern Rockies, upper Midwest and Northeast.

j. Runoff

The trend in annual R arises from the integrated interactions and trends of other terrestrial storage and fluxes components. Figure 13a shows the mean annual trend in total R, estimated as the sum of the NCA-LDAS surface and subsurface R variables. Mean annual

457 R is consistent with increasing mean annual P trends (Figure 4b), with increased R in the
458 Northeast, Midwest, and upper Great Plains. Decreasing trends in R are observed throughout
459 the Northwest, Southwest, and sporadically in the Southeast, also similar to the mean annual
460 P trend. One notable exception is the region of the central and southern Great Plains, where a
461 positive trend in R is observed. For Nebraska and Kansas, this can be explained mostly by
462 the increase trend in P shown in Figure 4b, although for Texas, the increased streamflow is
463 also consistent with the reduced ET trend previously shown in Figure 8a. Evaluating the
464 NCA-LDAS R trend is difficult due to the lack of observed natural streamflow, unimpacted
465 by anthropogenic impoundments and withdrawals. As a surrogate, the statistical comparisons
466 of NCA-LDAS annual R trends were conducted, each against trends estimated from the
467 monthly USGS HUC8 (4 km) R product (https://waterwatch.usgs.gov/) shown in Figure 13b.
468 HUC8 R, estimated by merging historical streamflow data, stream gauge drainage areas, and
469 watershed boundaries, has been successfully used in previous grid-based evaluations (Xia et
470 al., 2016; Velpuri et al., 2013). Results are shown in Table 3. They indicate RMSE errors
471 ranging from 2.42 mm in the Midwest to 22.2 mm in the Southwest, with a CONUS wide
472 RMSE error of 16.1 mm.

473 An additional indicator that highlights how R distribution has changed is the trend in
474 annual variance of daily R is shown in Figure 15a. The results are consistent with the annual
475 precipitation extreme indicators shown in Figures 5a, b, c and d. Overall, results indicate
476 increasing variance in annual runoff in the eastern half of the U.S, except along the southern
477 Appalachian Mountains. Decreasing trends are predominant in the western states, with
478 mixed trends for the Rocky Mountain region. The results are generally consistent with the
479 precipitation variance plot shown in Figure 5c.

Two other indicators related to extreme runoff are the maximum and minimum runoff events in a year. Figures 15b and c depict trends in annual 7-day low and 3-day high total runoff, respectively (USEPA, 2016). Trends in annual low flows are not significant at $p<0.1$ in much of the US. Positive trends are evident along the East coast, while negtive trends are observed in Florida and along the Gulf Coast. The lack of any significant trend in the West may be associated with the low end constraint of zero discharge. Increased trends in annual 3-day high flows, however, are significant across much of the Great Plains, upper Midwest, and in the East, except for the Appalachians. Results indicate positive trends in annual low and high flows along the East Coast, except for Florida, where low flows are decreasing and high flows are increasing. The NCA-LDAS trend patterms demonstrate consistency with those previously reported by Peterson et al., (2013) and Georgakakos et al. (2014).

k. Reference Period Using Thiel-Sen Estimator

The above results were presented in terms of absolute units that, while useful for scientific analyses, may be less apparent for certain users. To more readily show the trend over the period of analysis, absolute changes are often compared to an earlier reference period (Melillo et al., 2014). Here the intercept of the Thiel-Sen estimator (Sen, 1968) is employed that avoids having to decide which reference period is most appropriate. The Thiel-Sen estimator (Sen, 1968) is based on a least-squares fit over the median that minimizes the impact of outliers. Use of the intercept as the reference database effectively bases the trend on the entire 36-year period, and avoids having to choose an arbitrary single year or average number of years that might be anomalous. It further averts having to compare to years prior to 1979 that are outside the simulation period.

Figures 16a and 16b show two examples, the percent change in mean annual

503 precipitation and latent heat flux over NCA-LDAS's entire 36-year satellite period,
504 respectively. These are similar to Figures 4b and 8a, except that each grid cell has been
505 normalized by the Theil-Sen intercept and multiplied by 100 to express as a percent. Only
506 significant trends are reported. The images more clearly highlight the change over the 1980-
507 2015 satellite era. For instance, annual P in the Southwest has decreased from 0.9 to 1.2
508 %/yr compared to the median trend of that region, while the Upper Great Plains have
509 experienced an increase in P of about that same magnitude. Portions of the Northeast and
510 Midwest have experienced an increase in P of about 0.6 to 0.9 %/yr. Similarly, the Southwest
511 has experienced a decrease in ET of 0.9 to 1.2 %/yr, while the eastern half of the U.S. shows
512 increases in ET throughout, ranging up to 0.6 %/yr along the eastern states, and up to 0.9
513 %/yr percent in the Upper Great Plains, Midwest and South.

514 # 4. Discussion

515 ### *a) Assessment of NCA-LDAS Trends*

516 Overall, the NCA-LDAS mean annual hydrology trends demonstrate good consistency
517 between the forcing variables and other land surface components. For instance, increasing
518 trends in P and heavy precipitation in the Northern Great Plains, Midwest, and Northeast, are
519 reflected in increased trends in R and flooding in the Upper Missouri, and Ohio Rivers, and
520 major northeast rivers (E.g. Connecticut, Hudson, Susquehanna), respectively, consistent
521 with Peterson et al. (2013). Large positive trends in Rnet throughout the eastern US and
522 negative trends throughout the Southwest, are largely reflected by corresponding trends in
523 ET and EF in those same respective regions. Decreasing P further decreases ET in the
524 moisture limited Southwest. The decreasing trend in SCD throughout the US is impacted by

severe decreasing trends in P in the Southwest and increasing T and Rnet in the East.

Table 3 summarizes the NCA-LDAS RMSE for ET, SCD and R for each NCA region. For instance, the RMSE for mean annual ET trend ranged from a low of 0.05 $W/m^2/yr$ in the Northeast to a high of 0.21 $W/m^2/yr$ in the Midwest. This range is in fact about the same magnitude as the domain-wide ET trend from (Figure 8a) that ranged +/- 0.05 to 0.25 $W/m^2/yr$ and yields an overall 36-year change of +/- 1.8 to 9.0 W/m^2. These two measures arise from two separate sources; RMSE a comparison with independent data, and Mann-Kendall trend from an analysis of time series variability without comparison to ground truth. Similarly, the NCA-LDAS mean annual SCD trend RMSE ranged from a low of 1.15 days/yr in the Northeast to a high of 3.85 days/yr in the Great Plains. The domain wide SCD trend range of +/- 0.4 to 2.0 days/yr shown in Figure 10a yields an overall 36-year change of +/- 14.4 to 72.0 days. For R, the RMSE was about 3 mm/yr for the Northeast, Southeast and Midwest. For these regions, the R trends range from 3 to 12 mm/yr or 108 to 432 mm over 36 years. For the Great Plains and Southwest regions, a high RMSE of 12.3 to 22.0 mm is observed.

At the regional level, the ET trends from NCA-LDAS and FLUXNET showed good agreement over the overlapping 1983-2008 period. One major exception was the upper Midwest states of Illinois, Wisconsin, Iowa and Minnesota, where Figures 8a and b exhibited contrasting trends for NCA-LDAS and FLUXNET, respectively. While many factors contribute to ET, the difference is most likely due to NCA-LDAS's use of monthly climatological vegetation parameters, including greenness fraction, that preclude landcover change trends. Recent analyses of the AVHRR based Normalized Difference Vegetation Index (NDVI) by Scheftic et al. (2014) for 1982-2008 show a positive trend in duration of

548 growing season throughout much of the US, except in the Midwest Corn Belt that exhibits a
549 negative trend. They attribute the decreasing growing season to the expansion of agriculture
550 that has a shorter growing period compared to natural vegetation.

551 The SCD trends compared favorably in direction with Harpold's analyses in 10 of 13
552 basins of the intermountain west region as shown in Figure 11. These basins represent about
553 half of the entire U.S. Rocky Mountains. Despite the excellent statistics, the NCA-LDAS
554 trends were about twice as large as Harpold's trends. The mean annual nationwide average
555 of 1.2 days/yr was also as high. Possible reasons for this are: inaccurate calibration of the
556 0.125^{o} grid cell values over complex terrain; diminished satellite sensitivity at high snow
557 depth, due to microwave sensor saturation (Luojus et al., 2016); and elevation bias of the
558 SNOTEL stations. There also may be underestimation of the in-situ analysis due to unequal
559 distribution of the station locations, most of which are in non-mountainous areas.

560 R trend errors are reasonable except in the Great Plains and Southwest. This is
561 attributed to the large impact of the NCA-LDAS irrigation scheme which occurs without any
562 consideration of irrigation source, be it groundwater or streamflow. As implemented, NCA-
563 LDAS adds substantial "forcing", unaccounted in the modeled water balance. For example,
564 NCA-LDAS irrigation simulation in several states shown in Figure 14, such as California's
565 Central Valley (~300 mm/yr), Nebraska (100 mm/yr), and northwest Texas (100 mm/yr),
566 represent 50%, 17% and 14% of average annual P, respectively. California, whose irrigation
567 withdrawals are greater than all other Southwest NCA regions combined, takes about one-
568 third of its supply from groundwater (Maupin et al., 2014). In the Great Plains, the
569 groundwater withdrawals in Kansas, Nebraska, and Texas are about 80%, 60%, and 31%,
570 respectively of total irrigation. For other areas such as Texas that rely also on surface water

withdrawals from lakes and rivers, streamflow is greatly reduced.

Further, the current analysis illustrates that trends computed over a shorter record tend to produce less significant coverage. This is particularly evident in the ET analyses in Figures 8a and 8b where the period of analyses reduced from 36 to 24 years, the SCD analyses in Figures 10a and b where the period of analysis reduced from 36 to 17 years, and in the SWE analyses in Figures 12a and b, where the period of analysis changed from 36 to 12 years.

b) Effect of Multivariate Assimilation on RMSE and Trend Detection

The effect of NCA-LDAS data assimilation is examined two ways. First, a comparison is made between the RMSE evaluations of the NCA-LDAS for ET, SCD, and R against independent data, to OL evaluations using the same approach, as shown in Table 3. For ET, when compared against independent FLUXNET-MTE data, NCA-LDAS showed mixed results. NCA-LDAS RMSE for ET, when compared to OL, showed only slight improvement in the Northwest and Southwest; no impact in the Northeast and Midwest: and slight degradations for Great Plains and Southeast. NCA-LDAS also exhibited only very slight improvement in CONUS-wide (RMSE from 0.17 to 0.16 $W/m^2/yr$). NCA-LDAS SCD trends provided a more robust result. When evaluated against CMC data, NCA-LDAS RMSE demonstrated improvement in 3 of 4 reporting regions. For CONUS, NCA-LDAS reduced RMSE from 3.13 to 2.89 days/yr. Comparison was not possible for the Southeast and Midwest due to insufficient significant CMC record. For streamflow the NCA-LDAS RMSE degraded in 4 of 5 regions. These degradations were greatest in the Great Plains and Southwest where the irrigation scheme (Kumar et al., 2018; Ozdogan et al., 2010) was applied the most, as shown in Figure 14, affecting the natural water balance.

Second, the impact of multivariate assimilation was evaluated with respect to "trend

detection" based on the change in significant trend area between NCA-LDAS and OL. Table 4 indicates that trend detection slightly improved for ET in 4 of 6 NCA regions. For SCD, NCA-LDAS had a large effect as significant area increased in all areas ranging from 9 to 13%. For R, trend detection was unaltered. CONUS-wide, the NCA-LDAS-OL significant areas for ET, SCD and R increased by 2%, 11% and 0%, respectively. While not indicating an improvement in trend accuracy, the positive changes imply a decrease in uncertainty for those grid cells, and arguably a measure of the impact of data assimilation.

While the overall effect of satellite assimilation is small, several factors contribute to the impact of NCA-LDAS on model trends and improved significant area. First, land surface energy and water balance processes constitute an integrated non-linear system. Although bias is removed from the two assimilated state variables (satellite SM and SD), it is still theoretically possible that small differences can arise between DA and OL modeled land variables due to their non-linear linkages with the above two state variables, leading to small differences between the OL and DA trends. Second, since the model forcing time series (P, incoming radiation, wind speed, atmospheric water vapor deficits) as well as the prescribed vegetation and soil type parameters are not altered, any difference between the original and corrected states during assimilation will have a corresponding effect on other processes such as ET, R, infiltration, that are link to those states. For instance, SM is assimilated only at the surface soil layer (top 5 cm), but its impact is propagated by infiltration physics into the deeper subsurface soil layers. Also, ET is a non-linear function not only of root zone soil moisture, but also the model forcings that affect moisture transport through the root zone. At the same time, non-linear R generation is occurring related to SM and snowmelt. That is, a unit of rainfall on dry soil may provide no R, while the same amount rain or snowmelt on

saturated soil will completely run off. Other contributing factors include the influence of the snow cover area satellite (SCA) constraint within the DA scheme can also impact on trend detection. Another factor is that the SD observations are assimilated only if the Interactive Multisensor Snow and Ice Mapping System (IMS) and the MODIS SCA observations both indicate non-zero snow values. Consequently, the non-linear relationship with modeled flux and store variables can theoretically induce some impact of DA on trends. Finally, since data assimilation systems including EnKF are designed to correct the random error in the model background, while not altering the trend direction, the reduced variance in the time series can promote an improvement in trend "detection" as manifested in the increased significant area shown in Table 4 at $p<0.1$ used in this study. For NCA-LDAS, this can be attributed to both the theoretical reduction in random error associated with the snow depth bias reduction within EnKF, as well as the implementation of the IMS/MODIS snow cover detection algorithm. Finally, unlike the OL, NCA-LDAS employs a demand-driven, sprinkler irrigation scheme that affects soil moisture content (Ozdogan et al; 2010). Although not DA per se, the implementation in NCA-LDAS affects ET and R which can further lead to divergence of the trend as the irrigation scheme is not at all included in the OL.

. 5. Conclusions

There is pressing need to develop consistent trend indicators to facilitate scientific understanding of national climate change. Land reanalysis has evolved as an effective tool to achieve this goal, by merging disparate datasets of multiscale, multisensor, in situ and satellite data within a data assimilation modeling environment. NCA-LDAS has shown high skill when compared to other land surface models, offering a compelling database for

640 constructing regional-scale national hydrologic trends.

641 Analyses of annual mean hydrologic trends using NCA-LDAS demonstrate the
642 interrelationship between regional gradients in forcing trends, and trends in other land energy
643 and water stores and fluxes. Mean annual precipitation trends range from +3 to +9 mm/yr in
644 the Upper Great Plains and Northeast to -1 to -9 in the West and South; net radiation flux
645 trends range from +0.05 to +0.20 $W/m^2/yr$ in the East to -0.05 to -0.20 in the West; U.S.-
646 wide temperature trends average about +0.03K/yr.

647 Trends in the response water balance components, including annual mean soil moisture,
648 snow cover, latent and sensible heat fluxes and runoff are consistent with forcings. For
649 instance, increasing trends in P and heavy precipitation in the Northern Great Plains,
650 Midwest, and Northeast, are reflected, respectively, in increased trends in R in the Upper
651 Missouri and Ohio Rivers, as well as major northeast rivers, consistent with previous reports.
652 Large positive trends in Rnet and P throughout the eastern US and negative trends throughout
653 the Southwest, are largely reflected by corresponding trends in ET, and an increasing
654 evaporative fraction trend from West to East. The decreasing trend in SCD throughout the
655 US is impacted by severe decreasing trends in P in the Southwest, increasing Rnet in the
656 East, and elevated T throughout the US.

657 Evaluation of NCA-LDAS trends compared to independent data at the regional scale
658 indicates mixed results. The RMSE of CONUS-wide trends in number of snow cover days
659 improved from 3.13 to 2.89 days/yr while trend detection increased 11%; Trends in latent
660 heat flux were hardly affected, RMSE decreasing only 0.17 to 0.16 $W/m^2/yr$, while trend
661 detection increased 2%; NCA-LDAS runoff trends degraded significantly from 2.6 to 16.1
662 mm/yr while trend detection was unaffected.

663 The implication for the current analyses is that the West and Southwest are trending to
664 increasingly drier conditions under a climatically moisture-limited system, while the East and
665 North behave as energy-limited systems, trending toward more temperate conditions.
666 Regions of sparse significant forcing trends often result in reduced significant trends in other
667 hydrologic components, as evidenced by the central Great Plains.

668 At the regional level, the ET trends from NCA-LDAS and FLUXNET demonstrated
669 good agreement for the overlapping 1983-2008 period. One major exception was the upper
670 Midwest states where NCA-LDAS's use of monthly climatological vegetation parameters for
671 this area are not consistent with the decreasing growing season due to the expansion of
672 agriculture.

673 The SCD trends compared favorably in direction with Harpold's analyses using in situ
674 data in 10 of the 13 basins of the intermountain west region as shown in Figure 11. These
675 basins represent about half of the entire U.S. Intermountain West. Despite the excellent
676 statistics, the NCA-LDAS trends were about twice as large as Harpold's trends while the
677 mean annual nationwide average of 1.2 days/yr was also high. Possible reasons for this may
678 be inaccurate calibration of the 0.125^{o} grid cells over this complex terrain; diminished
679 satellite sensitivity at high snow depth, and non-representative distribution of the station
680 locations, most of which appear in non-mountainous areas. R trend errors are reasonable
681 except in the Great Plains and Southwest where the impact of NCA-LDAS irrigation is high.
682 As currently implemented, NCA-LDAS adds substantial "forcing", unaccounted in the
683 modeled water balance that needs to be addressed in future NCA-LDAS versions.

684 Precipitation station density analysis showed that satellite data assimilation improves
685 skill for soil moisture, streamflow and snow depth when precipitation station density is low,

686 while providing mixed results for higher precipitation station densities. This suggests that
687 there are possible limits to the effectiveness of data assimilation in regions with dense gage
688 networks.

689 Use of the Theil-Sen Estimator as a reference level offers an effective normalizing
690 method for comparing trends over a given period, and avoids having to choose an arbitrary
691 single year or average number of years that might be anomalous. For satellite-based
692 reanalysis, it further averts having to compare to databases that are outside the simulation
693 period.

694 The overall results demonstrate NCA-LDAS's capability as an effective enabling tool
695 for merging diverse satellite data products that can quantify physically consistent terrestrial
696 climate trends for scientific understanding and decision support. Data products are produced
697 not only for the principal hydrology components, but for a total of 42 variables as shown in
698 Table 5, and available for formulation of other indicators.

699 NCA-LDAS's long-term goal is to optimally combine the full suite of past and future
700 Earth observations of all relevant land EDRs. Future work will include observations
701 associated with terrestrial water storage, vegetation and altimetry. At the same time, the
702 results herein implicitly illustrate that employing the highest quality forcing dataset is still of
703 paramount importance to producing good hydrologic indicators. This notion provides
704 impetus for improving capability both in the accuracy and resolution of current satellite state
705 observations, and also for expanding space observations to include other fluxes such as
706 surface winds, H and ET.

707

708 ***Data Archive***

709 Details of NCA-LDAS documentation, data products, and visualization tools, several access
710 methods and other information are available on the NCA-LDAS Data Product Landing Page
711 or; http://disc.sci.gsfc.nasa.gov/datacollection/NCALDAS_NOAH0125_D_001.html.

712 ***Acknowledgements***

713 We are grateful to Dr. Allison Leidner of the Earth Science Division, NASA Headquarters,
714 and two anonymous reviewers, for their thoughtful comments on the submitted manuscript.
715 Research is supported by the NASA Earth Science Division in support of the National
716 Climate Assessment (NCA) of the U.S. Global Change Research Program (USGCRP).

References

Aguilar E., I. Auer, M. Brunet, M., T. C., Peterson, and J. Wieringa, 2003: Guidelines on climate metadata and homogenization. WMO/TD No. 1186, 50 pp.

Albergel, C., and Coauthors, 2013: Skill and global trend analysis of soil moisture from reanalyses and microwave remote sensing. *J. Hydrometeorol.*, 14, 1259–1277, doi:10.1175/JHM-D-12-0161.1.

Albergel, C., and Coauthors, 2017: Sequential assimilation of satellite-derived vegetation and soil moisture products using SURFEX_v8.0: LDAS-Monde assessment over the Euro-Mediterranean area. *Geosci. Model Dev.*, 10, 3889-3912, https://doi.org/10.5194/gmd-10-3889-2017.

Alemohammad, S. H., and Coauthors, 2017: Water, Energy, and Carbon with Artificial Neural Networks (WECANN): A statistically-based estimate of global surface turbulent fluxes using solar-induced fluorescence. *Biogeosciences*,, doi:10.5194/bg-14-4101-2017.

Baldocchi, D., and Coauthors, 2001: FLUXNET: A New Tool to Study the Temporal and Spatial Variability of Ecosystem–Scale Carbon Dioxide, Water Vapor, and Energy Flux Densities. *Bull. Am. Meteorol. Soc.*, **82**, 2415–2434, doi:10.1175/1520-0477(2001)082<2415:FANTTS>2.3.CO;2.

Barbu, A. L., J.-C. Calvet, J.-F. Mahfouf, and S. Lafont, 2014: Integrating ASCAT surface soil moisture and GEOV1 leaf area index into the SURFEX modelling platform: a land data assimilation application over France. *Hydrol. Earth Syst. Sci.*, 18, 173-192, https://doi.org/10.5194/hess-18-173-2014.

Barrett, A. P., 2003: National Operational Hydrologic Remote Sensing Center Snow Data Assimilation System (SNODAS) Products at NSIDC. NSIDC Special Report 11, 19 pp.

740 Bengtsson, L., S. Hagemann, and K. I. Hodges, 2004. Can climate trends be calculated from
741 reanalysis data? *Journal of Geophysical Research*, 109, D11111,
742 https://doi.org/10.1029/2004JD004536
743 Bierbaum, R., and Coauthors, 2014: Ch. 28: Adaptation. *Climate Change Impacts in the*
744 *United States: The Third National Climate Assessment*, J. M. Melillo, T. C. Richmond,
745 and G. W. Yohe, Eds., U.S. Global Change Research Program, 670-706,
746 doi:10.7930/J07H1GGT.
747 Blunden, J., and D. S. Arndt, Eds., 2013: State of the Climate in 2012. *Bull. Amer. Meteor.*
748 *Soc.*, **94**, S1–S238, doi:10.1175/2013BAMSStateoftheClimate.1.
749 Bonan, G. B., P. J. Lawrence, K. W. Oleson, S. Levis, M. Jung, M. Reichstein, D. M.
750 Lawrence, and S. C. Swenson, 2011: Improving canopy processes in the Community
751 Land Model version 4 (CLM4) using global flux fields empirically inferred from
752 FLUXNET data, *J. Geophys. Res.*, **116**, G02014, doi:10.1029/2010JG001593.
753 Boni, G., D. Entekhabi, and F. Castelli, 2001: Land data assimilation with satellite
754 measurements for the estimation of surface energy balance components and surface
755 control on evaporation. *Water Resour. Res.*, ***37***, 1713–1722,
756 doi:10.1029/2001WR900020.
757 Brocca, L., T. Moramarco, F. Melone, W. Wagner, S. Hasenauer, and S. Hahn, 2012:
758 Assimilation of surface- and root-zone ASCAT soil moisture products into rainfall–
759 runoff modeling. *IEEE T. Geosci. Remote*, **50**, 2542–2555,
760 doi:10.1109/TGRS.2011.2177468.
761 Brown, R. D., and B. Brasnett, 2015 (updated annually): Canadian Meteorological Centre
762 (CMC) Daily Snow Depth Analysis Data at National Snow and Ice Data Center,

763 Environment Canada.
764 Brown, R., C. Derksen, and L. Wang, 2010: A multi-data set analysis of variability and
765 change in Arctic spring snow cover extent, 1967–2008, *J. Geophys. Res.*, 115, D16111,
766 doi:10.1029/2010JD013975.
767 Burakowski, E. A., C. P. Wake, B. Braswell, and D. P. Brown, 2008: Trends in wintertime
768 climate in the northeastern United States: 1965–2005, J. Geophys. Res., 113, D20114,
769 doi:10.1029/2008JD009870.
770 Chen, F., W. T. Crow, and D. Ryu, 2014: Dual forcing and state correction via soil moisture
771 assimilation for improved rainfall–runoff modeling. *J. Hydrometeorol.*, **15**, 1832–1848,
772 doi:10.1175/JHM-D-14-0002.1.
773 Chen, M., W. Shi, P. Xie, V. B. S. Silva, V. E. Kousky, R. W. Higgins, and J. E. Janowiak,
774 2008: Assessing objective techniques for gauge-based analyses of global daily
775 precipitation. *J. Geophys. Res.*, **113**, D04110, doi:10.1029/2007JD009132.
776 Cohen, S. and G. Stanhill, G., 2016: Widespread surface solar radiation changes and their
777 effects: dimming and brightening. In: Letcher, T. (Ed.) Climate Change Observed
778 Impacts on Planet Earth, 2nd edition. Amsterdam: Elsevier, pp. 491–511.
779 Daly, C., R. P. Neilson, and D. L. Phillips (1994), A statistical-topographic model for
780 mapping climatological precipitation over mountainous terrain, J. Appl. Meteorol.,33,
781 140–158, doi:10.1175/1520-0450(1994)033<0140: ASTMFM>2.0.CO;2.
782 Dee, D., and Coauthors, 2011: The ERA-Interim reanalysis: Configuration and performance
783 of the data assimilation system. *Quart. J. Roy. Meteor. Soc.*, **137**, 553–597.
784 Dee, D. P., M. Balmaseda, G. Balsam, R. Engelen, A. J. Simmons, and J. N. Thepaut, 2014:
785 Toward a consistent reanalysis of the climate system. *Bull. Amer. Meteor. Soc.*, 95,

1235–1248, https://doi.org/10.1175/BAMS-D-13-00043.1.

De Lannoy, G. J. M., P. de Rosnay, and R. H. Reichle, 2015: Soil Moisture Data Assimilation. *Handbook of Hydrometeorological Ensemble Forecasting*, Q. Duan, F. Pappenberger, J. Thielen, A. Wood, H. L. Cloke, and J. C. Schaake, Eds., Springer Verlag, 1-43, doi:10.1007/978-3-642-40457-3_32-1.

Dorigo, W., R. De Jeu, D. Chung, R. Parinussa, Y. Liu, W. Wagner and D. Fernández-Prieto, 2012: Evaluating global trends (1988–2010) in harmonized multi-satellite surface soil moisture. *Geophys. Res. Lett.*, **39**, L18405 (2012).

Easterling, D.R., K.E. Kunkel, J.R. Arnold, T. Knutson, A.N. LeGrande, L.R. Leung, R.S. Vose, D.E. Waliser, and M.F. Wehner, 2017: Precipitation change in the United States. In: *Climate Science Special Report:Fourth National Climate Assessment, Volume I* [Wuebbles, D.J., D.W. Fahey, K.A. Hibbard, D.J. Dokken, B.C. Stewart, and T.K. Maycock (eds.)]. U.S. Global Change Research Program, Washington, DC, USA, pp. 207-230, doi: 10.7930/J0H993CC.

Ek, M., K. Mitchell, L. Yin, P. Rogers, P. Grunmann, V. Koren, G. Gayno, andJ. Tarpley, 2003: Implementation of Noah land-surface model advances in the NCEP operational mesoscale Eta model. Journal of Geophysical Research, **108 (D22)**,doi:10.1029/2002JD003 296.

Feng, H., and M. Zhang, 2015: Global land moisture trends: drier in dry and wetter in wet over land. *Sci. Rep.*, **5**, 18018-18023, doi:10.1038/srep18018.

Forman, B. A., and R. H. Reichle, 2013: The spatial scale of model errors and assimilated retrievals in a terrestrial water storage assimilation system. *Water Resour. Res.*, **49**, 7457–7468, doi:10.1002/2012WR012885.

809 Galantowicz, J. F., D. Entekhabi, and E. G. Njoku, 1999: Tests of sequential data
810 assimilation for retrieving profile soil moisture and temperature from observed L-band
811 radiobrightness. *IEEE T. Geosci. Remote*, **37**, 1860–1870, doi:10.1109/36.774699.
812 Georgakakos, A., P. Fleming, M. Dettinger, C. Peters-Lidard, T. C. Richmond, K. Reckhow,
813 K. White, and D. Yates, 2014: Ch. 3: Water Resources. *Climate Change Impacts in the*
814 *United States: The Third National Climate Assessment*, J. M. Melillo, T. C. Richmond,
815 and G. W. Yohe, Eds., U.S. Global Change Research Program, 69-112,
816 doi:10.7930/J0G44N6T.
817 Girotto, M., G. J. M. De Lannoy, R. H. Reichle, and M. Rodell, 2016: Assimilation of
818 gridded terrestrial water storage observations from GRACE into a land surface model.
819 *Water Resour. Res.*, **52**, 4164–4183, doi:10.1002/2015WR018417.
820 Girotto, M., G. J. M. De Lannoy, R. H. Reichle, M. Rodell, C. Draper, S. N. Bhanja, and A.
821 Mukherjee, 2017: Benefits and pitfalls of GRACE data assimilation: A case study of
822 terrestrial water storage depletion in India, *Geophys. Res. Lett.*, *44*, 4107–
823 4115,doi:10.1002/2017GL072994.
824 Global Change Research Act of 1990, Pub. L. 101-106, 104 STAT. 3096, 15 USC 2921-61.
825 Grotjahn, R., and J. Huynh, 2018: Contiguous US summer maximum temperature and heat
826 stress trends in CRU and NOAA Climate Division data plus comparisons to reanalyses.
827 *Scientific Reports*, 8:11146, doi:10.1038/s41598-018-29286-w.
828 Harpold, A., P. Brooks, S. Rajagopal, I. Heidbuchel, A. Jardine, and C. Stielstra, 2012:
829 Changes in snowpack accumulation and ablation in the intermountain west. *Water*
830 *Resour. Res.*, **48**, W11501, doi:10.1029/2012WR011949.
831 Hausfather, Z., K. Cowtan, M. J. Menne, and C. N. Williams Jr., 2016: Evaluating the impact

of U.S. Historical Climatology Network homogenization using the U.S. Climate Reference Network, *Geophys. Res. Lett.*, **43**, 1695-1701, doi:10.1002/2015GL067640.

Helsel, D.R. and R. M. Hirsch, 2002: Chapter A3: Statistical Methods in Water Resources. *Techniques of Water Resources Investigations of the United States Geological Survey: Book 4, Hydrologic Analysis and Interpretation*, U.S. Geological Survey, 522 pp.

Higgins, R.W., W. Shi, E. Yarosh and R. Joyce, 2000: Improved United States precipitation quality control system and analysis. NCEP/Climate Prediction Ctr. ATLAS No. 7, 40 pp.

Hori, M.,, K. Sugiura, K. Kobayashi, T. Aoki, T. Tanikawa, K. Kuchiki, M. Niwano, H. Enomoto, 2017: A 38-year (1978–2015) Northern Hemisphere daily snow cover extent product derived using consistent objective criteria from satellite-borne optical sensors, Remote Sens. Environ., 191 (2017), pp. 402-418, 10.1016/j.rse.2017.01.023.

Jacoby, H. D., and Coauthors, 2014: Ch. 27: Mitigation. *Climate Change Impacts in the United States: The Third National Climate Assessment*, J. M. Melillo, T. C. Richmond, and G. W. Yohe, Eds., U.S. Global Change Research Pogram, 648-669. doi:10.7930/J0C8276J.

Janetos, A. C., and Coauthors, 2012: National Climate Assessment Indicators: Background, Development, & Examples. No. PNNL-21183, 59pp, doi:10.2172/1128659

Jasinski, M., and Coauthors, 2014: "NCA-LDAS: NCA-LDAS: An Integrated Terrestrial Water Analysis System for Development, Evaluation, and Dissemination of Climate Indicators, Abstract GC51B-0405 presented at 2014 Fall Meeting, AGU, San Francisco, Calif., 15-19 Dec.

Jasinski, M., and Coauthors, 2015: "NCA-LDAS: An Integrated Terrestrial Water Analysis System for the National Climate Assessment - Sustained Assessment, Enabling Tools

855 Review, June 22, 2015,
856 https://weather.msfc.nasa.gov/NASA_NCA/internal/June2015/Jasinski_NCA%20LDAS
857 %20Mtg_062215_final2.pdf, 24 pp.
858 Jung, M., M. Reichstein, and A. Bondeau, 2009: Towards a global empirical upscaling of
859 FLUXNET eddy covariance observations: validation of a model tree ensemble approach
860 using a biosphere model. *Biogeosciences*, **6**, 2001–2003, doi:10. 5194/bg-6-2001-2009.
861 Karl, T. R., J. T. Melillo, and T. C. Peterson, 2009: *Global Climate Change Impacts in the*
862 *United States*. T.R. Karl, J.T. Melillo, and T.C. Peterson, Eds. Cambridge University
863 Press, 189 pp.
864 Kendall, M. G., 1975: *Rank Correlation Methods*, 4th edition, Charles Griffin, London.
865 Khaki M., E. Forootan, M. Kuhn, J. Awange, A.I.J.M. van Dijk, M. Schumacher, Sharifi,
866 M.A., 2018: Determining water storage depletion within Iran by assimilating GRACE
867 data into the W3RA hydrological mode *Advances in Water Resources*, 114 , pp. 1-18.
868 Khaki, M., J. Awange, 2019: The application of multi-mission satellite data assimilation for
869 studying water storage changes over South America. *Sci. Total Environ.*, 647, pp. 1557-
870 1572.
871 Knowles, N., 2015: Trends in snow cover and related quantities at weather stations in the
872 conterminous United States. *J. Clim.*, **28**, 7518–28.
873 Krajewski, W. F., G. J. Ciach, and E. Habib, 2003: An analysis of small-scale rainfall
874 variability in different climatic regimes, *Hydrological Sci. J.*, **48**, 151–162.
875 Kumar, S., and Coauthors, 2006: Land Information System: An interoperable framework for
876 high resolution land surface modeling. *Environ. Modell. Softw.*, **21**, 1402–1415.
877 Kumar, S., R. Reichle, R. Koster, W. Crow, and C. Peters-Lidard, 2009: Role of subsurface

878 physics in the assimilation of surface soil moisture observations. *J. Hydrometeorol.*, **10**,
879 1534–1547, doi:10.1175/2010JHM1262.1.
880 Kumar, S. V., and Coauthors, 2014: Assimilation of remotely sensed soil moisture and snow
881 depth retrievals for drought estimation. *J. Hydrometerol.*, **15**, 2446-2469, doi:
882 http://dx.doi.org/10.1175/JHM-D-13-0132.1.
883 Kumar, S.V., M.F. Jasinski, D. Mocko, M. Rodell, J. Borak, B. Li, H.K. Beaudoing and C.D.
884 Peters-Lidard, 2018: NCA-LDAS land analysis: Development and performance of a
885 multisensor, multivariate land data assimilation system for the National Climate
886 Assessment, *J. Hydrometeor.*, https://doi.org/10.1175/JHM-D-17-0125.1
887 Kunkel, K. E., M. Palecki, K. G. Hubbard, D. A. Robinson, K. T. Redmond, and D. R.
888 Easterling, 2007: Trend identification in twentieth-century U.S. snowfall: The
889 challenges. *J. Atmos. Ocean. Tech.*, **24**, 64–73, doi:10.1175/JTECH2017.1.
890 Kunkel, K. E., M. Palecki, L. Ensor, K. G. Hubbard, D. Robinson, K. Redmond, and D.
891 Easterling, 2009: Trends in twentieth-century U.S. snowfall using a quality-controlled
892 dataset. *J. Atmos. Ocean. Tech.*, **26**, 33–44, doi:10.1175/2008JTECHA1138.1.
893 Kunkel, K. E., D. A. Robinson, S. Champion, X. Yin, T. Estilow, and R. M. Frankson, 2016:
894 Trends and extremes in Northern Hemisphere snow characteristics. *Current Climate*
895 *Change Reports*, *2*(2), 65–73. doi.org/10.1007/s40641-016-0036-8.
896 Lee, J., S. Li, and R. Lund, 2014: Trends in extreme United States temperatures. *J. Climate*,
897 27, 4209–4225, doi:10.1175/ JCLI-D-13-00283.1.
898 Liu, L., Y. Hong, C. N. Bednarczyk, B. Yong, M. A. Shafer, R. Riley, and J. E. Hocker,
899 2012: Hydro-Climatological Drought Analyses and Projections Using Meteorological
900 and Hydrological Drought Indices: A Case Study in Blue River Basin, Oklahoma. *Water*

Resour. Manag., **26**, 2761-2779. doi:10.1007/s11269-012-0044-y

Luojus, K., J. Pulliainen, R. Brown, C. Derksen, T. Smolander, J. Cohen, J. Ikonen, L. Mudryk, 2016: Assessment of the satellite and model-based SWE datasets with snow transect reference data, Snowpex. [Available online at http://calvalportal.ceos.org/documents/10136/490405/Tue1.2.Luojus.pdf.]

Ma, N., G.-Y. Niu, Y. Xia, X. Cai, Y. Zhang, Y. Ma, and Y. Fang, 2017: A systematic evaluation of Noah-MP in simulating land-atmosphere energy, water, and carbon exchanges over the continental United States. Journal of Geophysical Research: Atmospheres, 122, 12,245–12,268. https://doi.org/10.1002/ 2017JD027597

Mann, H. B. 1945: Non-parametric tests against trend. *Econometrica*, **13**, 163-171.

Maupin, M.A., J. F. Kenny, S. S. Hutson, J. K. Lovelace, N. L. Barber, and K. S. Linsey, K.S., 2014: Estimated use of water in the United States in 2010: *U.S. Geological Survey Circular 1405*, 56 p., doi.org/10.3133/cir1405.

McNally, A., and Coauthors, 2017: A land data assimilation system for sub-Saharan Africa food and water security applications. *Sci. Data,* **4,** 170012, doi:10.1038/sdata.2017.12.

Melillo, J. M., T. C. Richmond, and G. W. Yohe, 2014: *Climate Change Impacts in the United States: The Third National Climate Assessment*. U.S. Global Change Research Program, 841 pp. doi:10.7930/J0Z31WJ2.

Mesinger, F. and Coauthors, 2006: North American Regional Reanalysis. *Bull. Amer. Meteor. Soc*. 87, 343–360, https://doi.org/10.1175/BAMS-87-3-343.

Mitchell, K. and Coauthors, 2004: The multi-institution North American Land Data Assimilation System (NLDAS): Utilizing multiple GCIP products and partners in a continental distributed hydrological modeling system. *J. Geophys. Res.*, **109**, D07S90.

924 Moss, R., and Coauthors, 2014: Ch. 26: Decision Support: Connecting Science, Risk
925 Perception, and Decisions. *Climate Change Impacts in the United States: The Third*
926 *National Climate Assessment,* J. M. Melillo, T. C. Richmond, and G. W. Yohe, Eds.,
927 U.S. Global Change Research Program, 620-647. doi:10.7930/J0H12ZXG.
928 Mote, P. W., and D. Sharp, 2016: Update to data originally published in: Mote, P. W., A. F.
929 Hamlet, M. P. Clark, and D. P. Lettenmaier, 2005: Declining mountain snow¬pack in
930 Western North America. *Bull. Amer. Meteor. Soc.* **86,** 39–49. [Available online
931 https://www.epa.gov/climate-indicators/climate-change-indicators-snowpack.]
932 National Operational Hydrologic Remote Sensing Center, 2004: Snow Data Assimilation
933 System (SNODAS) data products at NSIDC. Boulder, CO: National Snow and Ice Data
934 Center. Digital media.
935 Niu, G.-Y., and Coauthors, 2011: The community Noah land surface model with
936 multiparameterization options (Noah-MP): 1. Model description and evaluation with
937 local-scale measurements. *J. Geophys. Res.*, 116, D12109, doi:10.1029/2010JD015139.
938 Ozdogan, M., M. Rodell, H. K. Beaudoing, and D. L. Toll, 2010: Simulating the effects of
939 irrigation over the United States in a land surface model based on satellite-derived
940 agricultural data. *J. Hydrometeorol.*, **11**, 171–184, doi:10.1175/2009JHM1116.1.
941 Park, J. and M. Choi, 2015: Estimation of evapotranspiration from ground-based
942 meteorological data and global land data assimilation system (GLDAS). *Stoch. Env. Res.*
943 *Risk. A.*, **29**, 1963-1992, doi:10.1007/s00477-014-1004-2.
944 Parr, D., G. Wang, and C. Fu, 2016: Understanding evapotranspiration trends and their
945 driving mechanisms over the NLDAS domain based on numerical experiments using
946 CLM4.5. *J. Geophys. Res. Atmos.*, **121**, 7729–7745, doi:10.1002/2015JD024398.

947 Peters-Lidard, C., S. Kumar, D. Mocko, and Y. Tian, 2011: Estimating evapotranspiration
948 with land data assimilation systems. *Hydrol. Processes*, **25**, 3979–3992,
949 doi:10.1002/hyp.8387.
950 Peterson, T. C., and Coauthors, 2008: Why weather and climate extremes matter. *Weather*
951 *and Climate Extremes in a Changing Climate. Regions of Focus: North America,*
952 *Hawaii, Caribbean, and U.S. Pacific Islands*, T. R. Karl et al., Eds., U.S. Climate
953 Change Science Program and the Subcommittee on Global Change Research, 11–33.
954 Peterson, T. C., and Coauthors, 2013: Monitoring and understanding changes in heat waves,
955 cold waves, floods and droughts in the United States: State of knowledge. *Bull. Amer.*
956 *Meteor. Soc.*, **94**, 821-834, doi:10.1175/ BAMS-D-12-00066.1.
957 Reichle, R.H., S.V. Kumar, S.P.P. Mahanama, R.D. Koster, and Q. Liu, 2010: Assimilation
958 of satellite-derived skin temperature observations into land surface models. *J.*
959 *Hydrometeorol.*, **11**, 1103–1122. doi:10.1175/2010JHM1262.1.
960 Reichle, R., D. McLaughlin, and D. Entekhabi, 2002: Hydrologic data assimilation with the
961 ensemble Kalman Filter. *Mon. Weather Rev.*, **130**, 103–114.
962 Rodell, M., and Coauthors, 2004: The Global Land Data Assimilation System, *Bull. Amer.*
963 *Meteor. Soc.*, **85**, 381-394, doi:10.1175/BAMS-85-3-381.
964 Rohde, R., and Coauthors, 2013. Berkeley Earth Temperature Averaging Process. *Geoinfor*
965 *Geostat: An Overview* 1:2.
966 Rutgers University Global Snow Lab, 2016: Area of extent data: North America (no
967 Greenland). Accessed January 2016. http://climate.rutgers.edu/snowcover.
968 Sawada, Y., and T. Koike, 2014: Simultaneous estimation of both hydrological and ecological
969 parameters in an ecohydrological model by assimilating microwave signal. *J. Geophys.*

970 *Res. Atmos.*, 119, 8839–8857, doi:10.1002/ 2014JD021536.
971 Sawada, Y., T. Koike, and J. P. Walker, 2015: A land data assimilation system for
972 simultaneous simulation of soil moisture and vegetation dynamics. *J. Geophys. Res.*
973 *Atmos.*, 120, 5910–5930, doi:10.1002/2014JD022895.
974 Scheftic, W., X. Zeng, P. Broxton, M. Brunke, 2014: Intercomparison of Seven NDVI
975 Products over the United States and Mexico. *Remote Sens.* **6**, 1057-1084.
976 Sen, P.K. 1968: "Estimates of the regression coefficient based on Kendall's tau", *J. American*
977 *Stat. Assoc.*, **63** (324):1379–1389, JSTOR 2285891, MR 0258201, doi:10.2307/2285891.
978 Simmons A. J., K. M. Willett P. D. Jones, P. W. Thorne D. P. Dee, 2010: Low frequency
979 variations in surface atmospheric humidity, temperature and precipitation: Inferences
980 from reanalyses and monthly gridded observational datasets. *J. Geophys. Res.* **115**:
981 D01110.
982 Slater, A., 2016: Surface solar radiation in North America: A comparison of observations,
983 reanalyses, satellite, and derived products, *J. Hydrometeorol.*, **17**, doi:10.1175/JHM-D-
984 15-0087 .1.
985 St-Hilaire, A, T.B.M.J. Ouarda, M. Lachance, B., Bobee B, J., Gaudet, and C., Gignac, 2003:
986 Assessment of the impact of meteorological network density on the estimation of basin
987 precipitation and runoff: a case study. *Hydrol. Proc.,* **17**, 3561–3580.
988 Sturm, M., B. Taras, G.E. Liston, C. Derksen, T. Jonas, and J. Lea, 2010: Estimating snow
989 water equivalent using snow depth data and climate classes, *J. Hydrometeorol.*, **11**,
990 1380–1394.
991 Su, C.-H., D. Ryu, W. Dorigo, S. Zwieback, A. Gruber, C. Albergel, R. H. Reichle, and W.
992 Wagner, 2016: Homogeneity of a global multisatellite soil moisture climate data record,

993 *Geophys. Res. Lett.*, *43*, 11,245–11,252, doi:10.1002/2016GL070458.
994 Thorne, P. and R. S. Vose, 2010: Reanalyses suitable for characterizing long-term trends Are
995 they really achievable? *Bull. Amer. Meteorol. Soc.* **91**, 353–361,
996 https://doi.org/10.1175/2009BAMS2858.1.
997 U.S. Environmental Protection Agency. 2016: *Climate change indicators in the United*
998 *States*. Fourth edition. EPA 430-R-16-004. www.epa.gov/climate-indicators.
999 U.S. Global Change Research Program, 2012: *The National Global Change Research Plan*
1000 *2012–2021: A Strategic Plan for the U.S. Global Change Research Program*. 132 pp.,
1001 The U.S. Global Change Research Program, Washington, DC, USA. [Available online
1002 https://downloads.globalchange.gov/strategic-plan/2012/usgcrp-strategic-plan-2012.pdf.]
1003 U.S. Global Change Research Program. 2017a: *The National Global Change Research Plan*
1004 *2012–2021: A Triennial Update*. 102pp., The U.S. Global Change Research Program,
1005 Washington, DC, USA. [Available online https://downloads.globalchange.gov/strategic-
1006 plan/2016/usgcrp-strategic-plan-2016.pdf.]
1007 U.S. Global Change Research Program, 2017b: *Climate Science Special Report: Fourth*
1008 *National Climate Assessment, Volume I* [Wuebbles, D.J., D.W. Fahey, K.A. Hibbard, D.J.
1009 Dokken, B.C. Stewart, and T.K. Maycock (eds.)]. U.S. Global Change Research
1010 Program, Washington, DC, USA, 470 pp., doi: 10.7930/J0J964J6.
1011 Velpuri, N., G. Senay, R. Singh, S. Bohms, J. Verdin, 2013: A comprehensive evaluation of
1012 two MODIS evapotranspiration products over the conterminous United States: using
1013 point and gridded FLUXNET and water balance ET, *Remote Sens. Environ*., 139, pp. 35-
1014 49, 10.1016/j.rse.2013.07.013.
1015 Villarini, G., P. V. Mandapaka, W. F. Krajewski, and R. J. Moore, 2008: Rainfall and

sampling uncertainties: A rain gauge perspective, *J. Geophys. Res.*, **113**, D11102, doi:10.1029/2007JD009214.

Walsh, J., and Coauthors, 2014: Ch. 2: Our Changing Climate. *Climate Change Impacts in the United States: The Third National Climate Assessment*, J. M. Melillo, Terese (T.C.) Richmond, and G. W. Yohe, Eds., U.S. Global Change Research Program, 19-67. doi:10.7930/J0KW5CXT.

Wild, M., 2012: Enlightening global diming and brightening. *Bull. Amer. Meteor. Soc.* **93**, 27-37.

Wild, M. and Coauthors, 2008: Measurements of GDB. Workgroup 1 report at the ISF International workshop on GDB, Ein Gedi, Isr.

Wilson, C. B., J. B. Valdes, and I. Rodriguez-Iturbe, 1979: On the influence of the spatial distribution of rainfall on storm runoff. *Water. Resour. Res.*, **15**, 321–328.

Xia, Y. and Coauthors, 2012a: Continental-scale water and energy flux analysis and validation for the North American Land Data Assimilation System project phase 2 (NLDAS-2): 1. Intercomparison and application of model products, *J. Geophys. Res.*, **117**, D03109, doi: 10.1029/2011JD016048.

Xia, Y., and Coauthors, 2012b: Continental-scale water and energy flux analysis and validation for North American Land Data Assimilation System project phase 2 (NLDAS-2): 2. Validation of model-simulated streamflow, *J. Geophys. Res.*, **117**, D03110, doi:10.1029/2011JD016051.

Xia, Y., and Coauthors, 2016: Basin-scale assessment of the land surface water budget in the National Centers for Environmental Prediction operational and research NLDAS-2 systems, *J. Geophys. Res. Atmos.*,121, 2750–2779, doi:10.1002/2015JD023733.

1039 Zaitchik, B.F., and M. Rodell, 2009: Forward-looking assimilation of MODIS-derived snow
1040 covered area into a land surface model. *J. Hydrometeorol.*, **10**, 130-148.
1041 Zaitchik, B.F., M. Rodell, and R.H. Reichle, 2008: Assimilation of GRACE terrestrial water
1042 storage data into a land surface model: results for the Mississippi River Basin. *J.*
1043 *Hydrometeorol.*, **9**, 535-548, doi:10.1175/2007JHM951.1.
1044 Zhang, X., L. Alexander, G. C. Hegerl, P. Jones, A. K. Tank, T. C. Peterson, B. Trewin, and
1045 F. W. Zwiers, 2011: Indices for monitoring changes in extremes based on daily
1046 temperature and precipitation data, *Wiley Interdiscip. Rev. Clim. Change*, **2**, 851–870.
1047

1048

Tables

Table 1. Basic characteristics of NCA-LDAS

Latitude extent	25°N to 53°N
Longitude extent	-125° to -67°
Spatial resolution	1/8th degree
Temporal resolution	Daily
Time step	15 min
Dimension	224 (lat) x 464 (lon)
Grid box center points	Lower left: 25.0626°N, -124.9375°E Upper right: 52.9375°N, -67.0625°E
Land surface model	Noah Version 3.3
Format	NetCDF-4
Forcing data	NLDAS Phase-2

Table 2. Satellite datasets that are assimilated in NCA-LDAS

Name	Variable / Data	Platform(s)	Years
ESA CCI	Surface soil moisture	Various	1979-2002
LPRM (AMSR-E)	Surface soil moisture	Aqua	2002-2011
SMOPS (ASCAT)	Surface soil moisture	Metop-A/B	2007-2015
SMOPS (SMOS)	Surface soil moisture	SMOS	2010-2015
SMAP (NSIDC)	Surface soil moisture	SMAP	2015
SMM/I	Snow depth	Various	1987-2002
AMSR-E	Snow depth	Aqua	2002-2011
AMSR2	Snow depth	GCOM-W1	2012-2015
IMS	Snow-covered area	Various	1997-2015
MODIS	Snow-covered area	Terra	2000-2015
MODIS	Irrigated area	Terra	1979-2015

Table 3. RMSE comparison of NCA-LDAS (DA) and Open Loop (OL), each evaluated against independent data (FLUXNET-MTE for ET; CMC for SCD; HUC8 for runoff)

Region	ET ($W/m^2/yr$)	SCD (days/yr)	Runoff (mm/yr)
Northeast			
OL	0.05	1.59	**2.11**
DA	**0.05**	**1.15**	2.70
Southeast			
OL	**0.125**	-	3.36
DA	0.14	-	**3.17**
Midwest			
OL	**0.21**	-	**1.72**
DA	0.21	-	2.42
Great Plains			
OL	**0.15**	**3.71**	**2.20**
DA	0.16	3.85	12.33
Northwest			
OL	0.15	2.28	**7.55**
DA	**0.11**	**2.04**	9.00
Southwest			
OL	0.20	4.05	**2.243**
DA	**0.15**	**3.49**	22.184
CONUS			
OL	0.17	3.13	**2.55**
DA	**0.16**	**2.89**	16.05

Table 4. Comparison of percent significant area (p<0.1) of trends in ET, SCD and Runoff for NCA-LDAS (DA) and Open Loop (OL), and their differences (DA-OL)

NCA Region		ET	SCD	Runoff
Northeast	*OL*	88	76	34
	DA	88	88	40
	DA-OL	**0**	**12**	**6**
Southeast	*OL*	76	59	8
	DA	78	72	8
	DA-OL	**2**	**13**	**0**
Midwest	*OL*	77	78	16
	DA	78	90	16
	DA-OL	**1**	**12**	**0**
Great Plains	*OL*	38	58	35
	DA	35	67	32
	DA-OL	**-3**	**9**	**-3**
Northwest	*OL*	42	61	23
	DA	47	72	23
	DA-OL	**5**	**11**	**0**
Southwest	*OL*	58	71	43
	DA	66	84	44
	DA-OL	**8**	**13**	**1**
CONUS	*OL*	58	66	28
	DA	60	77	28
	DA-OL	**2**	**11**	**0**

Table 5. NCA-LDAS variables available on GES-DISC.

Short Name	Long Name	Unit
Swnet	Net shortwave radiation flux	W m-2
Lwnet	Net longwave radiation flux	W m-2
Qle	Latent heat net flux	W m-2
Qh	Sensible heat net flux	W m-2
Qg	Heat flux	W m-2
Snowf	Snow precipitation rate	kg m-2 s-1
Rainf	Rain precipitation rate	kg m-2 s-1
Evap	Evapotranspiration	kg m-2 s-1
Qs	Storm surface runoff	kg m-2 s-1
Qsb	Baseflow-groundwater runoff	kg m-2 s-1
Qsm	Snow melt	kg m-2 s-1
RadT	Average radiative temperature	K
SWE	Snow depth water equivalent	kg m-2
SnowDepth	Snow depth	m
SnowFrac	Snow covered fraction	fraction
SoilMoist0_10cm	Soil moisture (0 - 10 cm)	m^3 m-3
SoilMoist10_40cm	Soil moisture (10 - 40 cm)	m^3 m-3
SoilMoist40_100cm	Soil moisture (40 - 100 cm)	m^3 m-3
SoilMoist100_200cm	Soil moisture (100 - 200 cm)	m^3 m-3
SoilTemp0_10cm	Soil temperature (0 -10 cm)	K
SoilTemp10_40cm	Soil temperature (10 - 40 cm)	K
SoilTemp40_100cm	Soil temperature (40 - 100 cm)	K
SoilTemp100_200cm	Soil temperature (100 -200 cm)	K
PotEvap	Potential evaporation rate	kg m-2 s-1
ECanop	Canopy water evaporation rate	kg m-2 s-1
TVeg	Transpiration rate	kg m-2 s-1
ESoil	Direct evaporation from bare soil	kg m-2 s-1
SubSnow	Snow sublimation rate	kg m-2 s-1
CanopInt	Plant canopy surface water	kg m-2
Streamflow	Streamflow	m^3 s-1
FloodedFrac	Flooded fraction	fraction
FloodedArea	Flooded area	m^2
IrrigatedWater	Irrigated water rate	kg m-2 s-1
Wind_f	Wind speed	m s-1
Rainf_f	Total precipitation rate	kg m-2 s-1
Tair_f	Temperature	K
Tair_f_min	Daily minimum temperature	K
Tair_f_max	Daily maximum temperature	K
Qair_f	Specific humidity	kg kg-1
Psurf_f	Pressure	Pa
SWdown_f	Downward shortwave radiation	W m-2
LWdown_f	Downward longwave radiation flux	W m-2

List of Figures

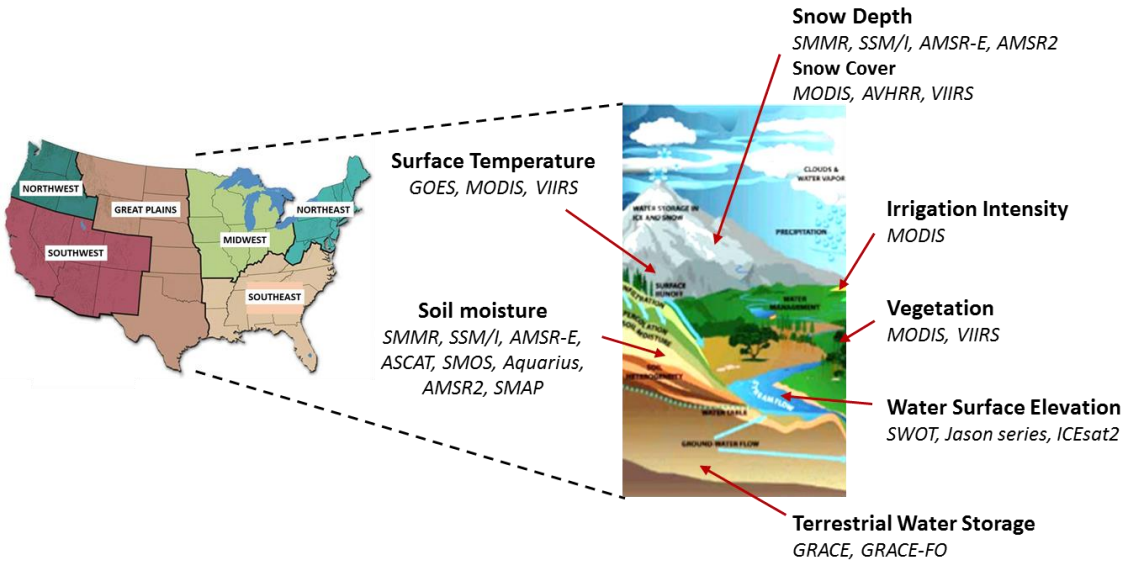

Figure 1. The long-term vision of NCA-LDAS is to optimally combine the full suite of all relevant past and future satellite EDRs to provide a high quality climatology of U.S. terrestrial hydrology. Satellite EDRs would include soil moisture, snow, land surface temperature, water surface elevation, vegetation, irrigation intensity and terrestrial water storage.

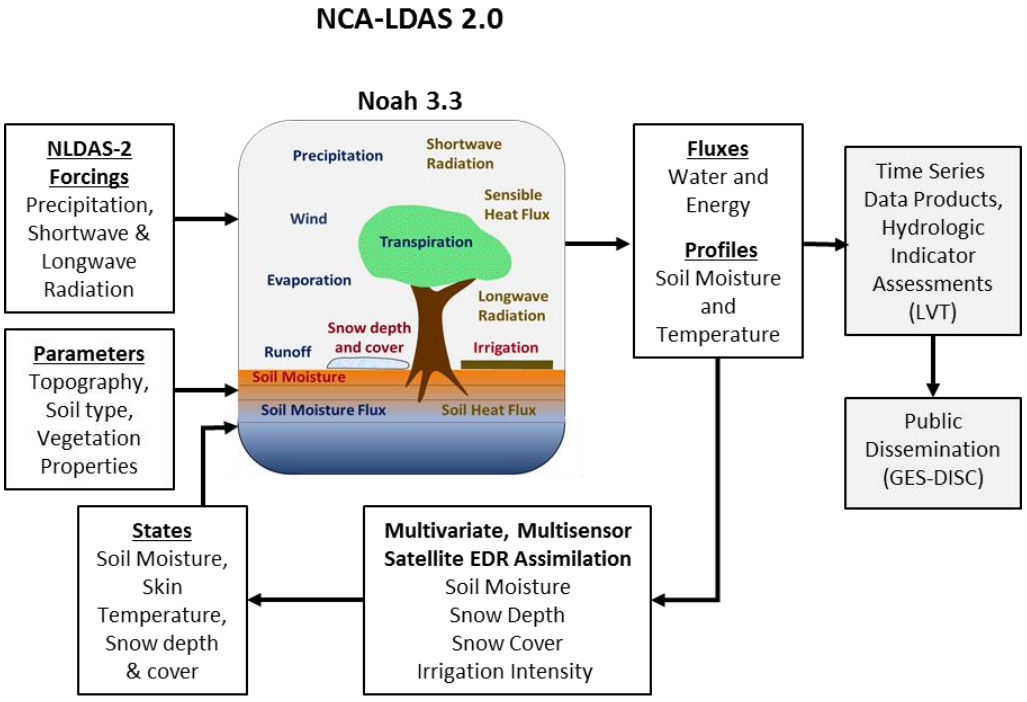

Figure 2. Schematic of NCA-LDAS Version 2.0. Built within LIS, NCA-LDAS adds the capability to assess trend indicators for any of the 42 input and output variables.

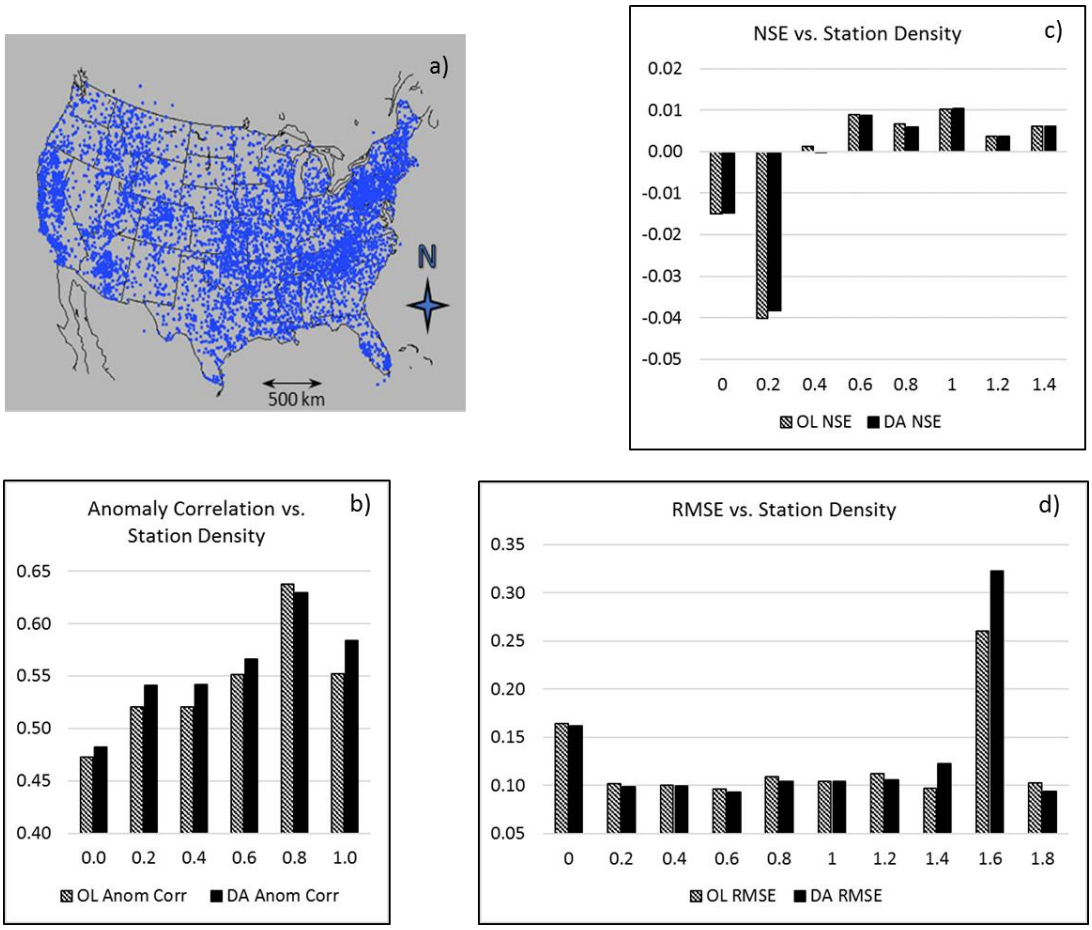

Figure 3. a) Typical CPC reporting stations for a single day (Higgins et al., 2000); Impact of CPC precipitation station density on NCA-LDAS evaluation for b) soil moisture, c) Nash Sutcliffe Efficiency normalized information contribution, and d) snow depth, where station density is the number of reporting gauges per NCA-LDAS 0.25 degree grid cell.

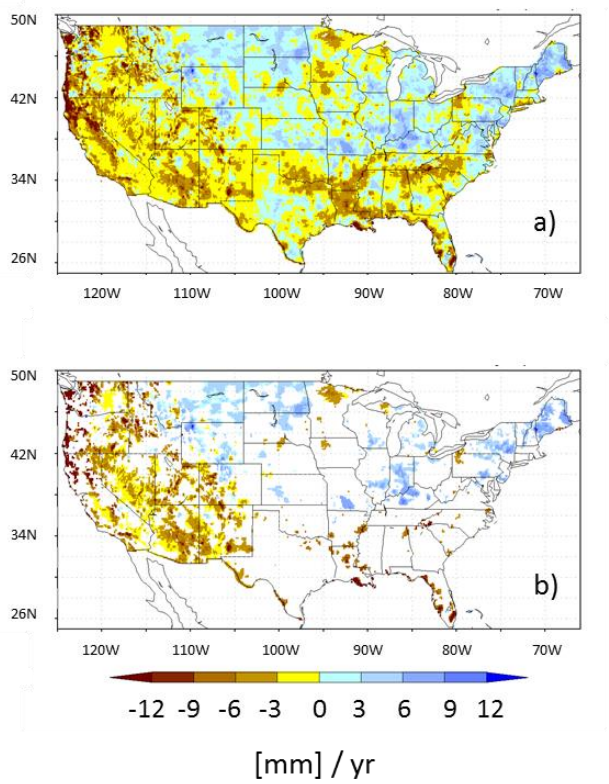

Figure 4. NCA-LDAS trends in annual precipitation for water year 1980-2015, for a) full model results and b) only for p<0.10.

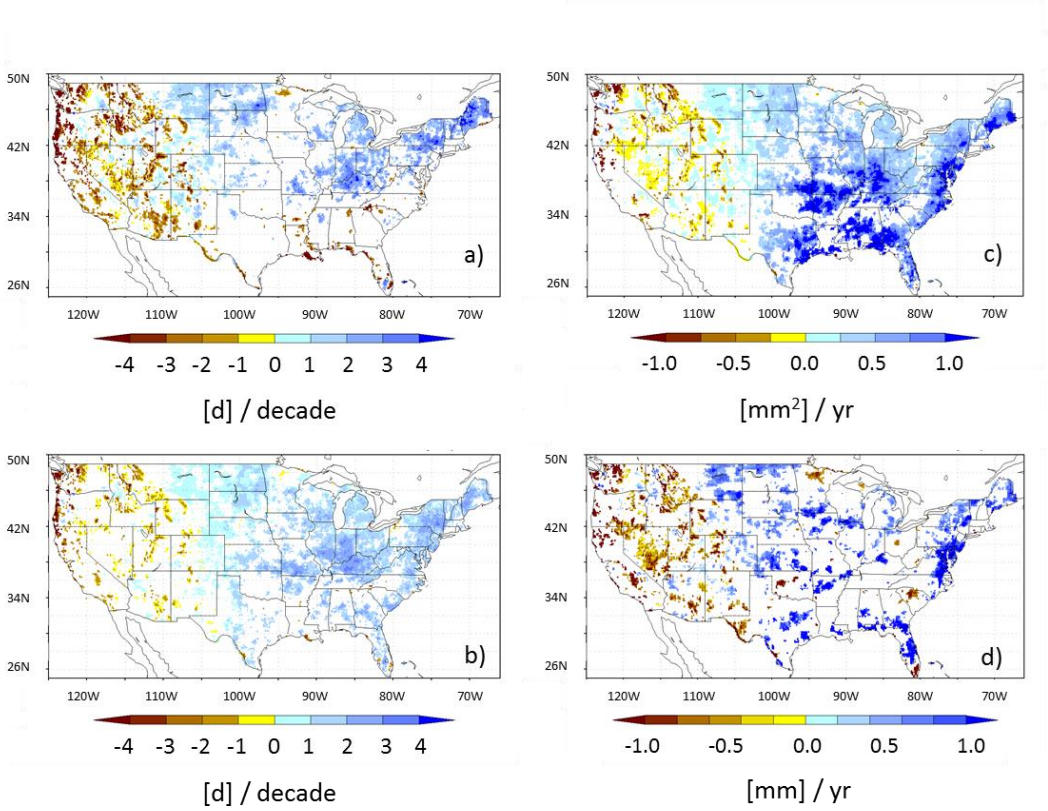

Figure 5. Trends in a) mean annual number of days of heavy precipitation (>10 mm), b) mean annual number of days of very heavy precipitation (>20 mm), c) variance in annual daily precipitation and d) 5-day high precipitation, for water year 1980-2015, p<0.10.

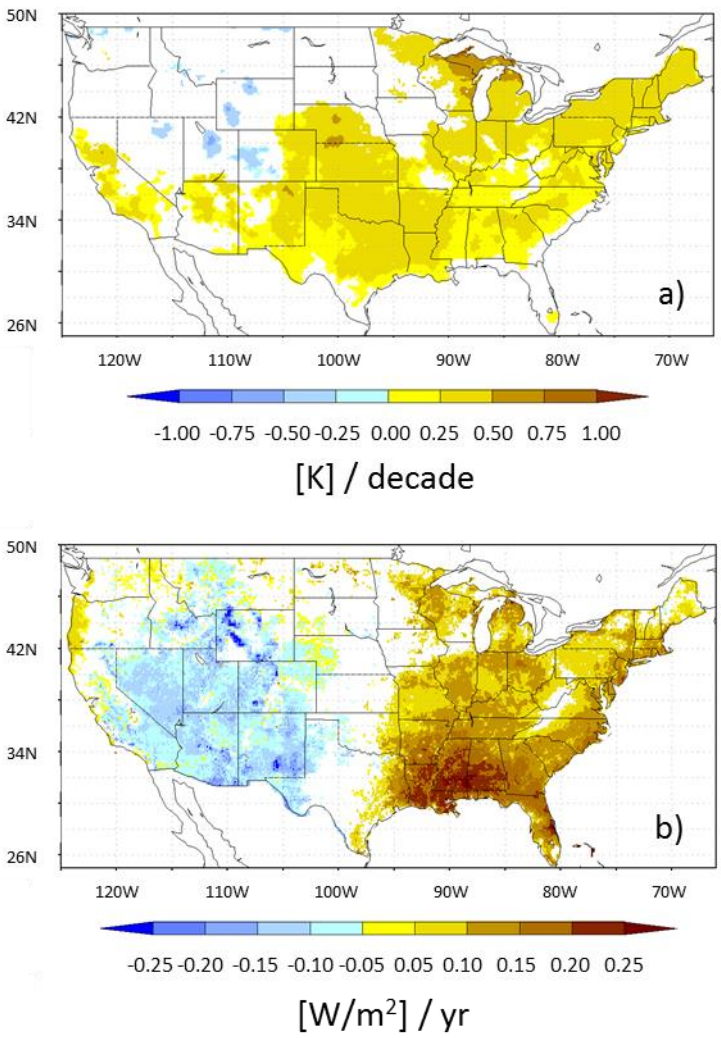

Figure 6. Trends in mean annual a) surface temperature, and b) net radiation, for 1980-2015, p<0.10.

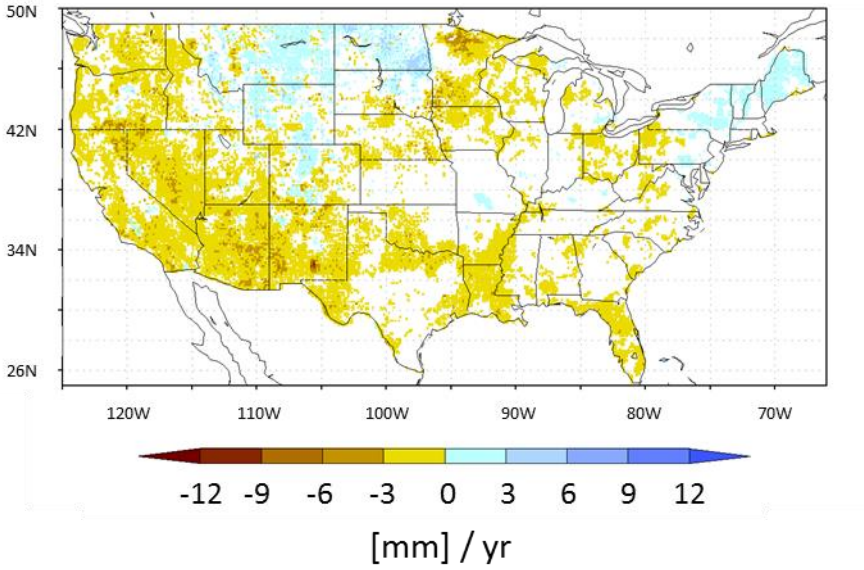

Figure 7. NCA-LDAS indicator for the trend in mean annual soil moisture for the period 1980-2015, p<0.10.

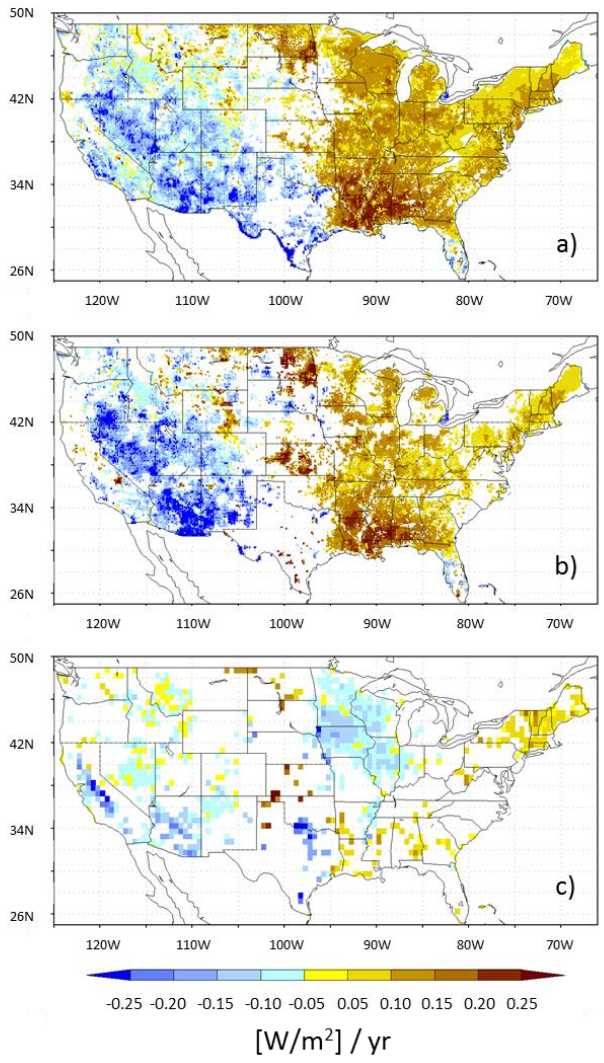

1230

1231 *Figure 8. Trend in mean annual ET, p<0.10, for a) entire NCA-LDAS simulation period 1980-*

1232 *2015, b) NCA-LDAS simulation period 1983-2008 that overlaps with FLUXNET-MTE, and c)*

1233 *FLUXNET-MTE period 1983-2008.*

1234

1235

1236

1237

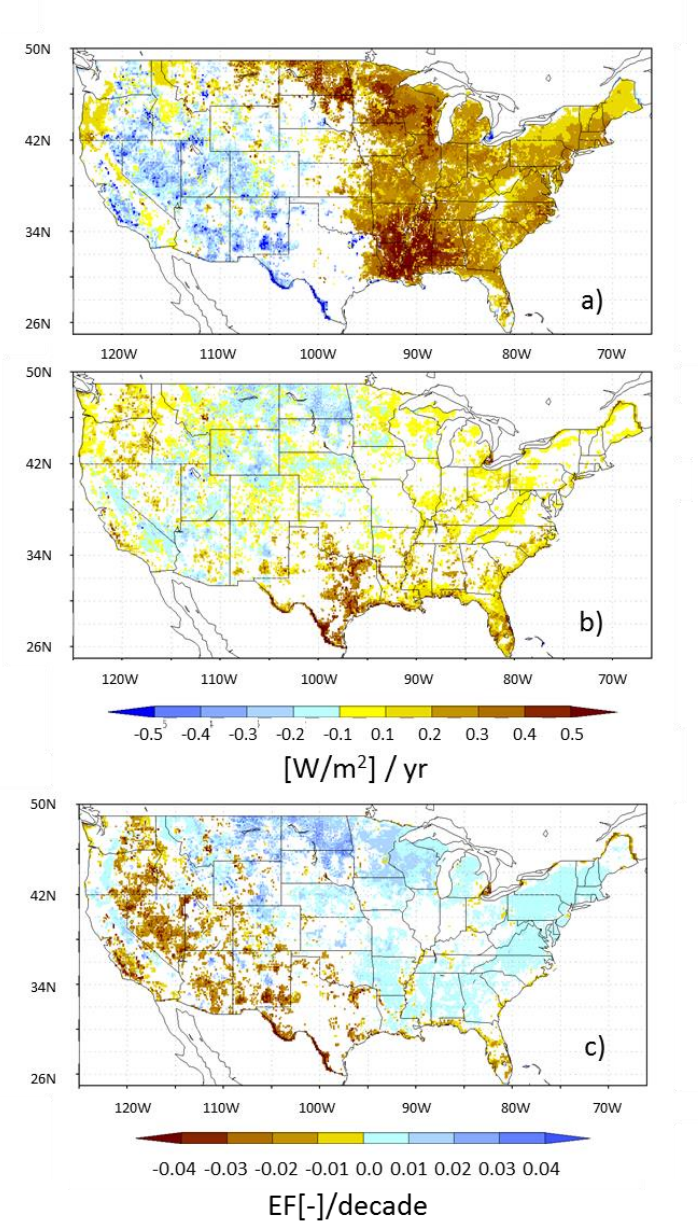

Figure 9. Trends in June-July-August for the period 1980-2015, p<0.10, for a) mean latent heat flux, b) mean sensible heat flux, and c) mean EF per decade.

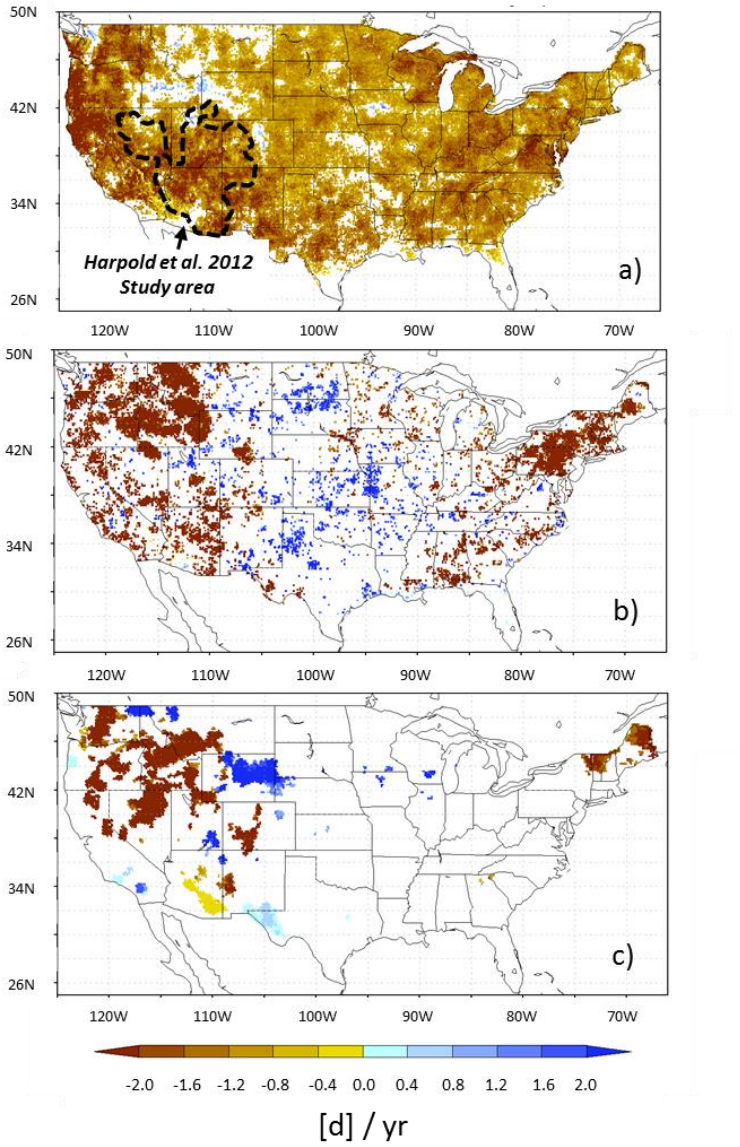

Figure 10. Trends in number of snow-covered days for a) NCA-LDAS period 1980-2015, b) NCA-LDAS period 1999-2015, and c) CMC snow cover period 1999-2015.

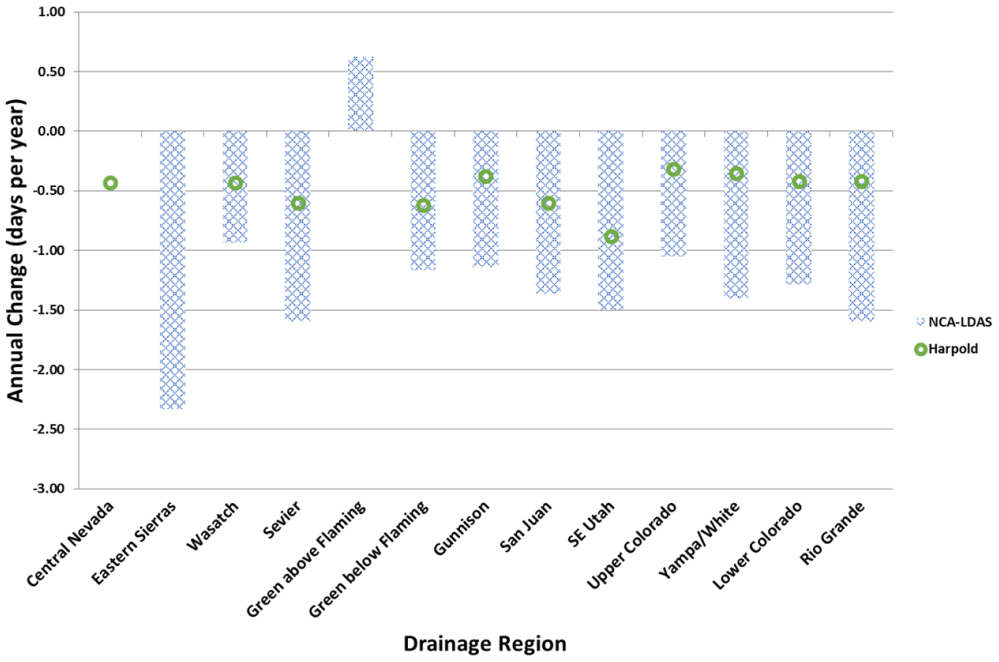

Figure 11. Evaluation of trend in number of days with snow on ground in intermountain west (blue bars), compared to Harpold et al., 2012 (green markers), FOR 1984-2009 with p<0.05.

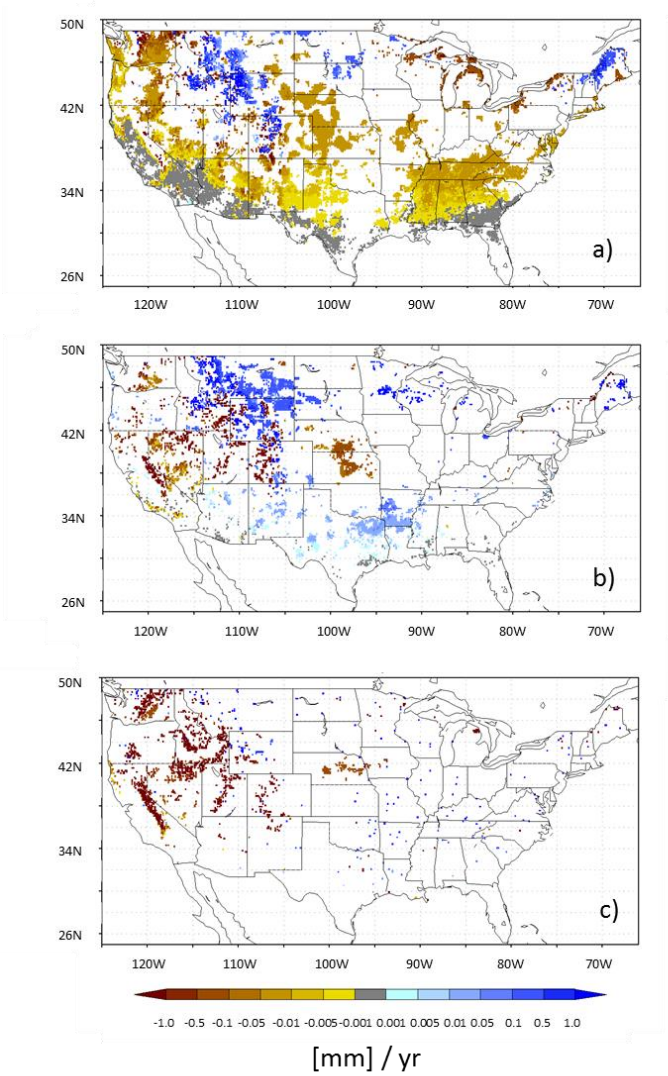

Figure 12. Trends in mean October-June SWE with 7-day smoothing, p<0.10, for a) full NCA-LDAS period, 1980-2015, b) NCA-LDAS 2004-2015, and c) same trend analyses for SNODAS data 2004-2015.

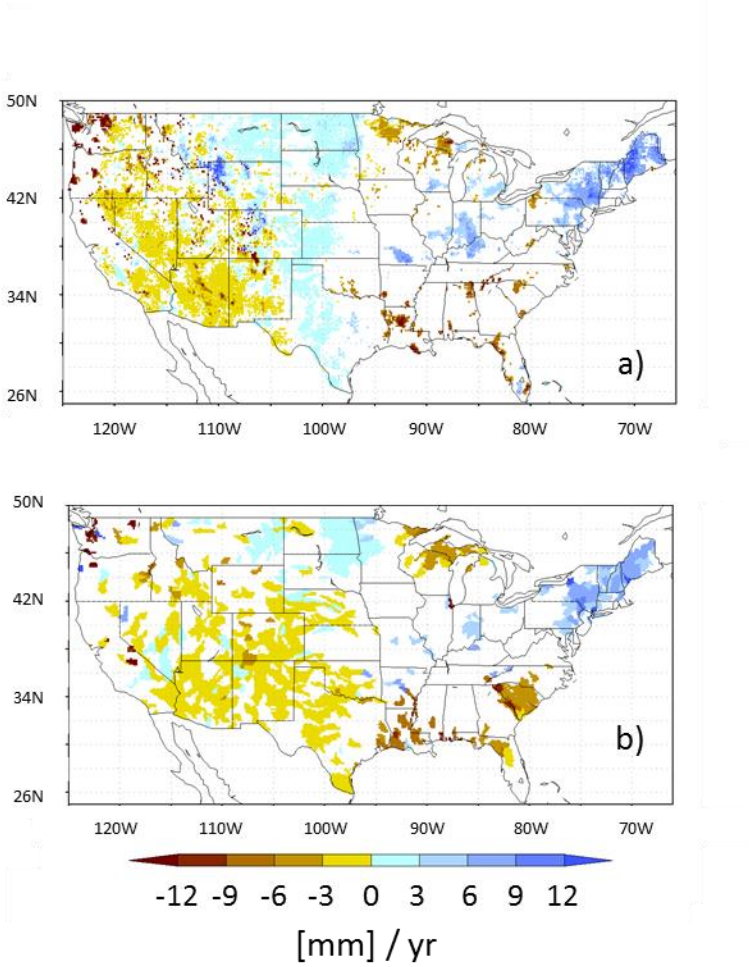

Figure 13. Mean annual runoff trends for period 1980-2015 at p<0.10, for a) NCA-LDAS and b) USGS HUC8.

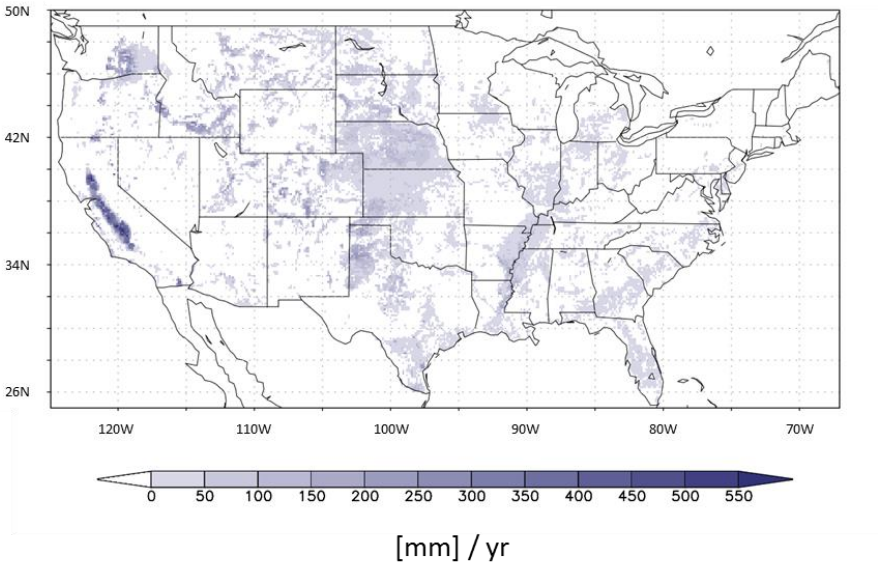

Figure 14. NCA-LDAS mean assimilated irrigation intensity over the period 1980-2015 (from Kumar et al., 2018).

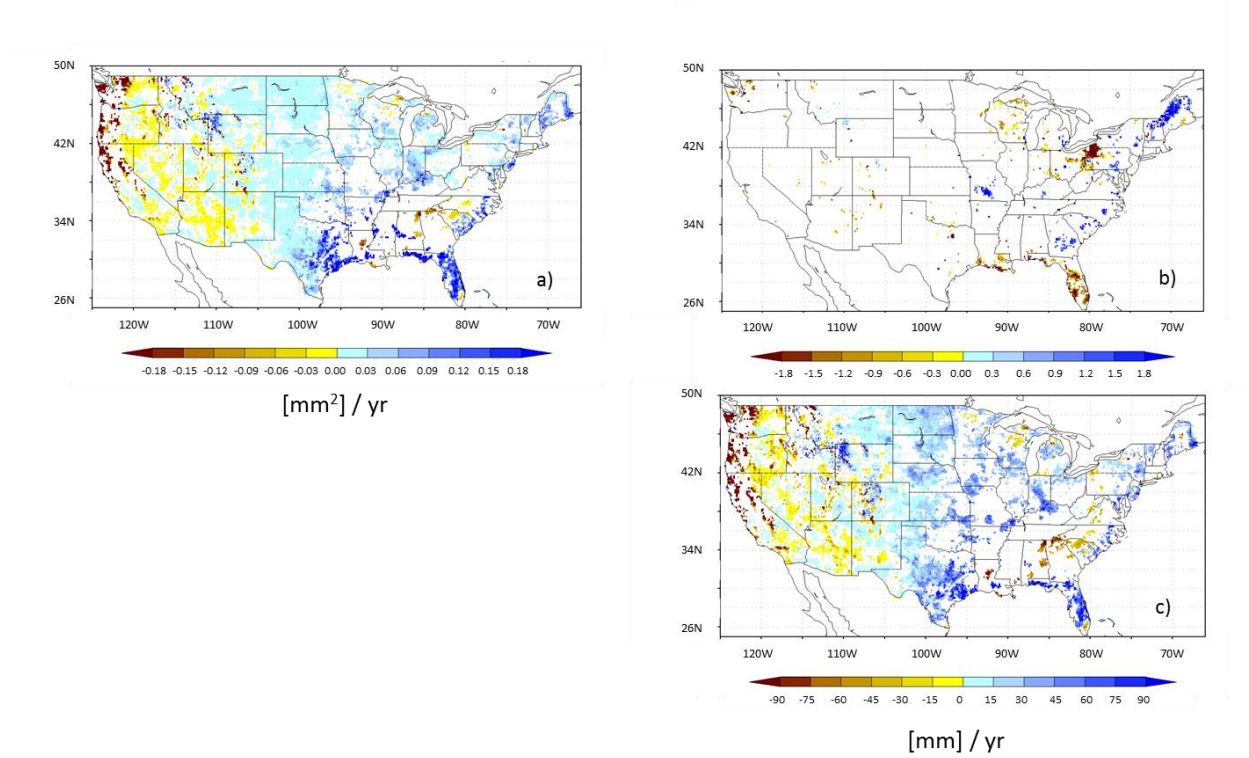

Figure 15. Trend in NCA-LDAS over 1980-2015 for a) variance in annual streamflow, b) annual 7-day low streamflow and c) annual 3-day high streamflow (USEPA, 2016).

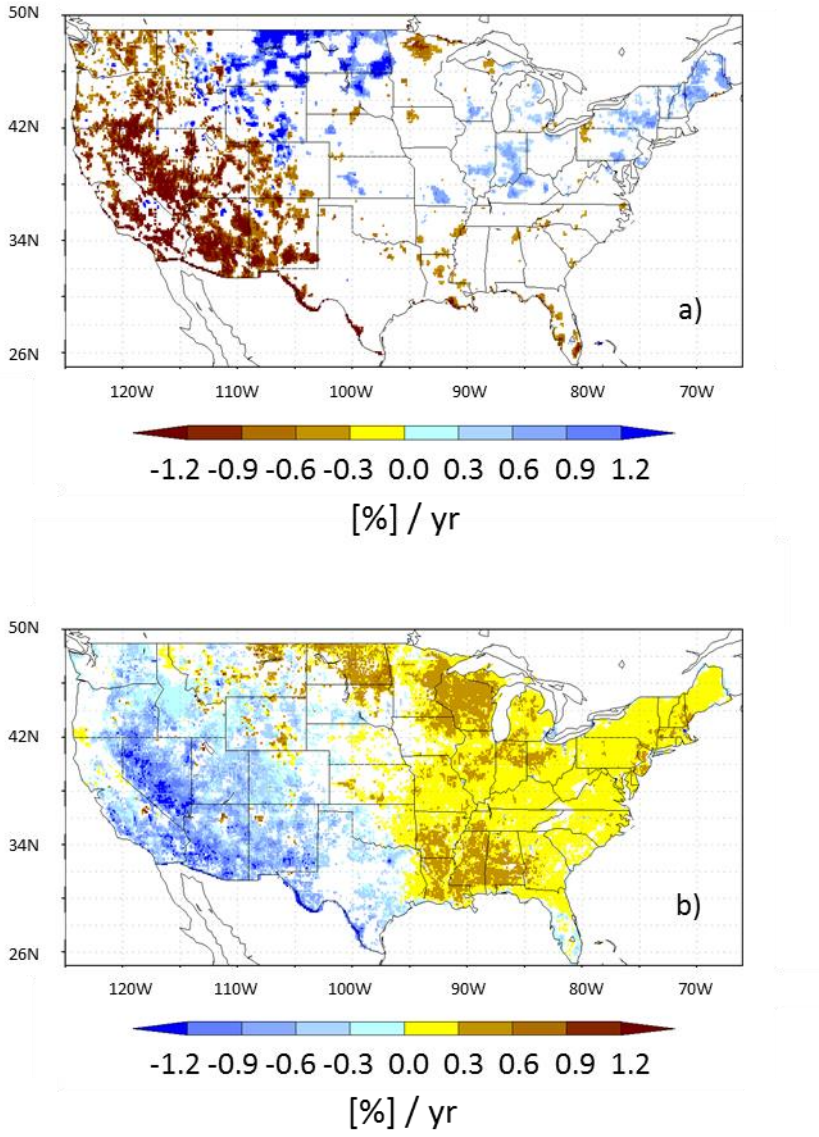

Figure 16. Percent change in a) mean annual precipitation, and b) mean annual latent heat flux, over the period 1980-2015, expressed with respect to intercept of the Theil-Sen Estimator, for p<0.1.

1309